NAVAL POSTGRADUATE SCHOOL

MONTEREY, CALIFORNIA

THESIS

COMPARISON OF DIFFERENT IMPLEMENTATION OPTIONS FOR DENSITY DISCONTINUITY IN SPLIT–STEP FOURIER PARABOLIC EQUATION MODELS

by

Matthew D. Owens

March 2014

Thesis Advisor: Kevin B. Smith
Second Reader: Daphne Kapolka

Approved for public release; distribution is unlimited

THIS PAGE INTENTIONALLY LEFT BLANK

REPORT DOCUMENTATION PAGE

Form Approved OMB No. 0704–0188

1. AGENCY USE ONLY ***(Leave blank)***	**2. REPORT DATE** March 2014	**3. REPORT TYPE AND DATES COVERED** Master's Thesis

4. TITLE AND SUBTITLE
COMPARISON OF DIFFERENT IMPLEMENTATION OPTIONS FOR DENSITY DISCONTINUITY IN SPLIT–STEP FOURIER PARABOLIC EQUATION MODELS

5. FUNDING NUMBERS

6. AUTHOR(S) Matthew D. Owens

7. PERFORMING ORGANIZATION NAME(S) AND ADDRESS(ES)
Naval Postgraduate School
Monterey, CA 93943–5000

8. PERFORMING ORGANIZATION REPORT NUMBER

9. SPONSORING /MONITORING AGENCY NAME(S) AND ADDRESS(ES)
N/A

10. SPONSORING/MONITORING AGENCY REPORT NUMBER

11. SUPPLEMENTARY NOTES The views expressed in this thesis are those of the author and do not reflect the official policy or position of the Department of Defense or the U.S. Government. IRB Protocol number ____N/A____.

12a. DISTRIBUTION / AVAILABILITY STATEMENT
Approved for public release; distribution is unlimited

12b. DISTRIBUTION CODE

13. ABSTRACT (maximum 200 words)

This paper studies alternate ways to model density discontinuity in split-step Fourier parabolic equation models. The Monterey-Miami Parabolic Equation model is used to implement an alternative to the effective index term in the smoothing function and a split-step Fourier/Finite Difference hybrid technique. The model is shown to converge to a stable solution that is slightly lower than the benchmark solution. A range step size of approximately one wavelength is shown to provide the closest approximation to the benchmark solution. Acceptable solutions are obtained with large depth grid sizes for the alternate smoothing function. Smaller depth grid sizes are necessary for accurate solutions when using the hybrid implementation technique. The effect of reference sound speed is shown to minimize the phase error present when the models are used in the presence of a strong density discontinuity.

14. SUBJECT TERMS Split-step Fourier, Parabolic Equation, Monterey-Miami Parabolic Equation, Finite Difference, Hybrid, Density Discontinuity

15. NUMBER OF PAGES 65

16. PRICE CODE

17. SECURITY CLASSIFICATION OF REPORT	**18. SECURITY CLASSIFICATION OF THIS PAGE**	**19. SECURITY CLASSIFICATION OF ABSTRACT**	**20. LIMITATION OF ABSTRACT**
Unclassified	Unclassified	Unclassified	UU

NSN 7540–01–280–5500

Standard Form 298 (Rev. 2–89)
Prescribed by ANSI Std. 239–18

THIS PAGE INTENTIONALLY LEFT BLANK

Approved for public release; distribution is unlimited

COMPARISON OF DIFFERENT IMPLEMENTATION OPTIONS FOR DENSITY DISCONTINUITY IN SPLIT–STEP FOURIER PARABOLIC EQUATION MODELS

Matthew D. Owens
Lieutenant, United States Navy
B.A., Virginia Polytechnic Institute and State University, 2006

Submitted in partial fulfillment of the
requirements for the degree of

MASTER OF SCIENCE IN APPLIED SCIENCE (ACOUSTICS)

from the

NAVAL POSTGRADUATE SCHOOL
March 2014

Author: Matthew D. Owens

Approved by: Kevin B. Smith
Thesis Advisor

Daphne Kapolka
Second Reader

Clyde Scandrett
Chair, Undersea Warfare Academic Group

THIS PAGE INTENTIONALLY LEFT BLANK

ABSTRACT

This paper studies alternate ways to model density discontinuity in split-step Fourier parabolic equation models. The Monterey-Miami Parabolic Equation model is used to implement an alternative to the effective index term in the smoothing function and a split-step Fourier/Finite Difference hybrid technique. The model is shown to converge to a stable solution that is slightly lower than the benchmark solution. A range step size of approximately one wavelength is shown to provide the closest approximation to the benchmark solution. Acceptable solutions are obtained with large depth grid sizes for the alternate smoothing function. Smaller depth grid sizes are necessary for accurate solutions when using the hybrid implementation technique. The effect of reference sound speed is shown to minimize the phase error present when the models are used in the presence of a strong density discontinuity.

THIS PAGE INTENTIONALLY LEFT BLANK

TABLE OF CONTENTS

THIS PAGE INTENTIONALLY LEFT BLANK

LIST OF FIGURES

LIST OF ACRONYMS AND ABBREVIATIONS

FD	finite-difference
FE	finite-element
FEPE	finite-element parabolic equation
FFT	fast Fourier transforms
MMPE	Monterey-Miami Parabolic Equation
PE	parabolic equation
SSF	split-step Fourier
TL	transmission loss
WAPE	wide-angle parabolic equation

THIS PAGE INTENTIONALLY LEFT BLANK

ACKNOWLEDGMENTS

I would like to thank Professor Smith for his patience and encouragement throughout the thesis writing process. I would not have been able to finish this without his guidance.

THIS PAGE INTENTIONALLY LEFT BLANK

I. INTRODUCTION

A. BACKGROUND

Parabolic equation (PE) methods have been used in the field of physics for many years to reduce the two-way, elliptic wave equation to a simpler, one-way equation. Although originally utilized in the field of plasma physics, Hardin and Tappert [1] were the first to introduce the PE method for solving underwater acoustic propagation in the early 1970s. The PE approximation to the wave equation is first order differential in range (r), and therefore was able to be numerically solved by using a one-way marching algorithm, such as the split-step Fourier (SSF) algorithm. The SSF technique works by first sampling the acoustic field on a depth grid, i.e., with uniform sampling Δz, at a single range r. The depth grid then undergoes two fast Fourier transforms (FFTs) and two vector multiplications in order to obtain the solution at the next range step $r + \Delta r$. The process is repeated at each range step until the entire acoustic field is modeled [2]. The major advantages of the SSF technique are its computational efficiency, stability, and simplicity.

Alternately, finite-difference (FD) techniques may be used to solve PEs. Numerical implementation of the FD algorithm is similar to SSF. The acoustic field is first specified at all depths at an initial range. A finite-difference approximation based on a Taylor series expansion of the derivative terms is then directly applied to the density-dependent, transverse differential operator. The solution is obtained by solving a tridiagonal system of equations with dimensions equal to the number of depth samples at each range step [3]. By directly applying the finite-difference approximation to each element in the depth mesh, the FD technique avoids having to use a smoothing function and can be used in a variety of ocean environments but at the cost of increased computational complexity.

A third method of solving PEs is the finite-element (FE) method. This method discretizes the ocean environment into multiple nodes using Galerkin's method [4]. Then by applying continuity of pressure and the normal component of particle velocity to the

boundary conditions of each node, a tridiagonal system of equations is established that can be solved through well-defined methods. By discretizing the environment, the FE method has the ability to increase or decrease the number of nodes within a local depth range, which leads to more detailed or faster calculations than possible by using FD techniques [5]. However, due to the complexity of FE schemes and their associated stability issues, FD and SSF techniques are the preferred method in the modeling community [6].

The 1981 PE Workshop [7] proved Harding and Tappert's SSF technique was able to efficiently and accurately model the acoustic field in long-range, narrow-angle problems with negligible bottom interactions. More advanced SSF methods based on higher-order operator splittings of the so-called "square root operator," such as introduced by Thomson and Chapman [8], also greatly improved the accuracy of the approach for wide-angle solutions.

In areas with strong bottom interactions, such as in shallow water, the SSF technique has been shown to be less accurate. This is due to the fact that the propagator term in the SSF algorithm contains density derivatives in the effective index of refraction term, which require the use of a smoothing function to approximate the density profile in the vicinity of the ocean bottom [9]. This accuracy of the smoothing function's approximation is considered to be the major weakness to SSF based models.

In 1997, Yevick and Thomson [10] proposed a hybrid SSF/FD method. Their initial motivation was to introduce a small set of equations (generally five) that treat the density discontinuity directly through a finite difference approximation rather than relying on the mixing function previously employed, thereby improving the accuracy of the solution. The remainder of the calculations and marching algorithm are performed via SSF techniques. This method capitalizes on the accuracy of the FD technique while utilizing the efficiency of a SSF marching algorithm. This method has shown accurate results and is efficient enough for use in two and three dimensions.

In addition, they were able to show some improved phase accuracy (through less sensitivity to the reference sound speed) by incorporating additional higher order terms in

the operator splitting of the square root operator. These additional terms were also shown to lend themselves to finite difference solutions. In this case, however, the application of the set of finite difference equations extended over the entire depth computational domain.

B. PROBLEM STATEMENT

The Monterey-Miami Parabolic Equation (MMPE) [11] method utilizes a SSF technique to model the propagation of the acoustic field underwater. Versions of MMPE have been developed for both 2-D and 3-D, single frequency and broadband calculations, and including various types of environmental fluctuations, such as internal waves, surface roughness, 3-D bathymetric variations, turbulence, and others. The MMPE model utilizes the wide-angle PE (WAPE) approximation of Thomson and Chapman [8], and deals with the density discontinuity by using a hyperbolic tangent mixing function approximation to the Heaviside step function at the bottom interface.

This model has been shown to be accurate in deep-ocean problems [12]. However, MMPE's treatment of the bottom condition can become problematic in shallow water environments where bottom interactions play a significant role. In this thesis, we will consider solutions to the acoustic propagation in a simple, Pekeris waveguide, where the environment is defined as having a lossless water column with constant sound speed of 1500 m/s and a bottom depth of 300 m, below which is a homogeneous half-space of sound speed 1700 m/s, density 1.5 g/cm3, and attenuation 0.5 dB/λ. The source is modeled as an omnidirectional point source at depth 180 m transmitting a single-frequency, continuous wave (CW) signal at 100 Hz. For comparison purposes, a transmission loss trace will be extracted at 100 m depth out to a maximum range of 20 km.

When compared to a coupled-mode model, known as Couple (and considered capable of generating benchmark quality solutions) and a finite-element parabolic equation (FEPE) model, the MMPE model is quite accurate at shorter ranges, as can be seen in Figure 1. However, at about 5 km a phase error begins to appear and accumulate as the range is increased. The objective of this work is to study multiple implementation

options for modeling the density discontinuity in MMPE in order to improve the model's long-range accuracy. Insights into the cause of this phase error accumulation with range will also be explored.

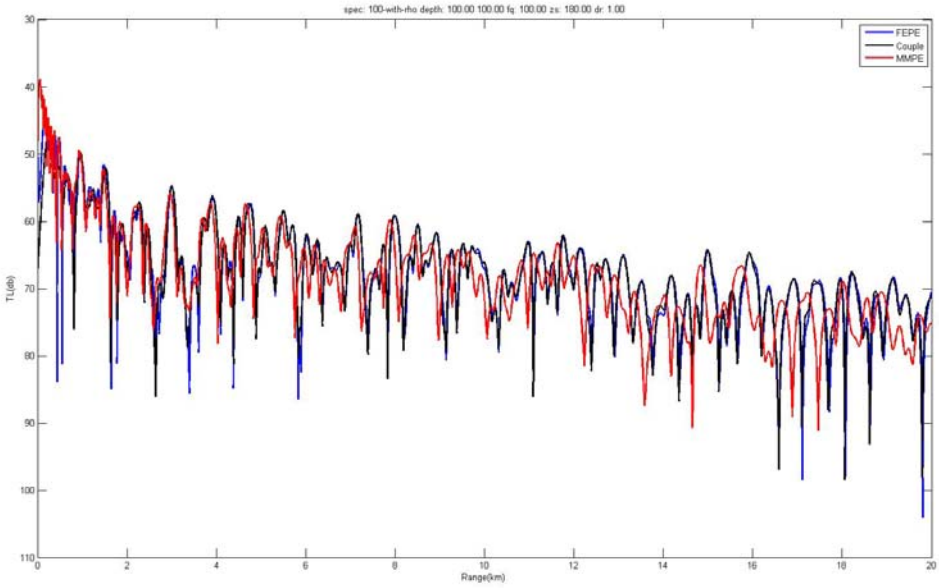

Figure 1. Plot of TL (dB) vs. Range for Couple, FEPE, and MMPE.

II. THEORY

A. PARABOLIC EQUATION DERIVATION

We begin with the Helmholtz equation for acoustic pressure, $p(r,z)$, in cylindrical coordinates for a time-dependent harmonic field,

$$\frac{1}{r}\frac{\partial}{\partial r}\left(r\frac{\partial p}{\partial r}\right)+\rho(z)\frac{\partial}{\partial z}\left(\frac{1}{\rho(z)}\frac{\partial p}{\partial z}\right)+k_0^2 n^2(r,z)\,p=0\,, \tag{1}$$

where $k_0=\dfrac{\omega}{c_0}$ is the reference wavenumber, $n(r,z)=\dfrac{c_0}{c(r,z)}$ is the acoustic index of refraction, c_0 is the reference sound speed, $c(r,z)$ is the acoustic sound speed, and $\rho(z)$ is the density (which is assumed to vary only with depth at any given range). It is within $c(r,z)$ and $\rho(z)$ that all features of the environment are represented.

If we now introduce the so-called PE field function according to

$$\Psi(r,z)=\frac{1}{\sqrt{k_0 r}}\,p(r,z)e^{-ik_0 r}\ , \tag{2}$$

and assume that the solution is dominated by the forward propagating field, it can be shown [9] that the 2-D Helmholtz equation can be reduced to a parabolic equation of the form

$$\frac{\partial\Psi}{\partial r}=ik_0(Q-1)\Psi\ , \tag{3}$$

where the square-root operator, Q, is defined as

$$Q=\sqrt{n^2+\frac{1}{k_0^2}\rho\frac{\partial}{\partial z}\left(\frac{1}{\rho}\frac{\partial}{\partial z}\right)}\ . \tag{4}$$

By defining the operators

$$\varepsilon = n^2 - 1$$
$$\mu = \frac{1}{k_0^2}\frac{\partial^2}{\partial z^2} \tag{5}$$
$$\gamma = -\frac{1}{k_0^2 \rho}\frac{\partial \rho}{\partial z}\frac{\partial}{\partial z}$$

the square-root operator may be written as

$$Q = \sqrt{1 + \varepsilon + \mu + \gamma} \ . \tag{6}$$

Solutions to the parabolic equation may then be obtained from a one-way marching algorithm solution in the general form

$$\Psi\left(r + \Delta r, z\right) = \exp\left[ik_0 \Delta r\left(Q - 1\right)\right]\Psi\left(r, z\right) \ . \tag{7}$$

In practice, it is not possible to directly apply the square-root operator in the marching algorithm defined above. Some form of approximation is required.

Alternatively, we could define the field function as

$$\widetilde{\Psi} = \sqrt{p}\Psi \ , \tag{8}$$

which then satisfies a PE of similar form

$$\frac{\partial \widetilde{\Psi}}{\partial r} = ik_0\left(\widetilde{Q} - 1\right)\tilde{\Psi} \ . \tag{9}$$

In this case, the square-root operator is defined by

$$\widetilde{Q} = \sqrt{\tilde{n}^2 + \frac{1}{k_0^2}\frac{\partial^2}{\partial z^2}} = \sqrt{1 + \tilde{\varepsilon} + \mu} \tag{10}$$

where

$$\tilde{\varepsilon} = \tilde{n}^2 - 1, \text{ and } \tilde{n}^2 = n^2 + \frac{1}{2k_0^2}\left[\frac{1}{\rho}\frac{\partial^2 \rho}{\partial z^2} - \frac{3}{2}\left(\frac{1}{\rho}\frac{\partial \rho}{\partial z}\right)^2\right] . \tag{11}$$

The original approaches in MMPE were based on this latter definition, which requires a description of $\rho(z)$ in terms of a mixing function to smooth out the discontinuity at the bottom interface so that the derivatives may be computed. The solution to this PE is also obtained from a marching algorithm of the form given in Equation (7).

B. APPROXIMATION OF THE SQUARE-ROOT OPERATOR

The Thomson-Chapman WAPE operator splitting [8] produces an approximation to the square-root operator in Equation (6), defined by [10]

$$Q_1' = \sqrt{1+\varepsilon} + \sqrt{1+\mu} + \sqrt{1+\gamma} - 2 \ . \tag{12}$$

By using this definition, the propagator in the marching algorithm becomes

$$\begin{aligned} &\exp\left[ik_0 \Delta r \left(Q_1' - 1 \right) \right] = \exp\left[i\delta \left(\sqrt{1+\varepsilon} + \sqrt{1+\mu} + \sqrt{1+\gamma} - 3 \right) \right] \\ &\approx \exp\left[i\delta \left(\sqrt{1+\gamma} - 1 \right) \right] \exp\left[i\delta \left(\sqrt{1+\mu} - 1 \right) \right] \exp\left[i\delta \left(\sqrt{1+\varepsilon} - 1 \right) \right] \\ &= \exp\left[i\delta \left(\sqrt{1+\gamma} - 1 \right) \right] \exp\left[i\delta \left(\sqrt{1+\mu} - 1 \right) \right] \exp\left[i\delta \left(n - 1 \right) \right] \end{aligned} \tag{13}$$

where $\delta \equiv k_0 \Delta r$, and the approximation in the 2nd line is due to the neglect of any non-commutation of the operators ε, μ, and γ. As noted by Yevick and Thomson [10], the order in which the operations are implemented is important, and the term with γ should be applied at the end of the range step. Note that the operator currently used in MMPE corresponds to

$$\tilde{Q}_1' = \sqrt{1+\tilde{\varepsilon}} + \sqrt{1+\mu} - 1 \quad , \tag{14}$$

and there is no γ term of concern.

The Thomson-Chapman approximation neglects the lowest order cross terms between the operators. The lowest order correction is [10]

$$\begin{aligned} Q_2' &= Q_1' - \frac{1}{8}\left[\left(\varepsilon + \mu + \gamma \right)^2 - \varepsilon^2 - \mu^2 - \gamma^2 \right] \\ &= Q_1' - \frac{1}{8}\left[\varepsilon \left(\mu + \gamma \right) + \left(\mu + \gamma \right) \varepsilon + \mu\gamma + \gamma\mu \right] \ . \end{aligned} \tag{15}$$

For completeness, note that the corresponding lowest order correction to the existing MMPE operator would be

$$\begin{aligned}\tilde{Q}_2' &= \tilde{Q}_1' - \frac{1}{8}\left[\left(\tilde{\varepsilon}+\mu\right)^2 - \tilde{\varepsilon}^2 - \mu^2\right] \\ &= \tilde{Q}_1' - \frac{1}{8}\left[\tilde{\varepsilon}\mu + \mu\tilde{\varepsilon}\right] \quad .\end{aligned} \tag{16}$$

In PE models based on the SSF algorithm, the operators containing ε (or $\tilde{\varepsilon}$) and μ are treated as simply scalar operators in the physical space (z) and wavenumber space $\left(k_z\right)$, respectively. The vector multiplication is then a trivial task, which leads to the great efficiency of the SSF approach. However, this does require that operators containing ε and μ are separated in the approximation of the square-root operator.

If we assume that the γ terms and cross terms can be added later as corrections, then an intermediate step solution can be defined as

$$\tilde{\Psi}\left(r+\Delta r, z\right) = FFT^{-1}\left[\exp\left\{i\delta\left(\sqrt{1-\frac{k_z^2}{k_0^2}}-1\right)\right\}\times FFT\left\{\exp\left[i\delta\left(n-1\right)\right]\Psi\left(r,z\right)\right\}\right]. \tag{17}$$

Note that if we replace n by $\tilde{n}$, then this is the complete range step utilized in the existing MMPE code.

C. DENSITY SMOOTHING APPROACH

In order to utilize the simpler approach in MMPE, based upon Equations (9), (10), (11), and (14), we must first define the mixing function for the density contrast. In this case, the density profile is defined in terms of a generalized function representing the discontinuity at the water-bottom interface by

$$\rho\left(z\right) = \rho_w + \left(\rho_b - \rho_w\right)\bar{H}\left(z - z_b\right), \tag{18}$$

where

$$\bar{H}\left(z-z_b\right) = \bar{H}\left(\varsigma\right) = \left(1+e^{-\varsigma/L}\right)^{-1} = \frac{1}{2}\left[1+\tanh\left(\frac{\varsigma}{2L}\right)\right] \tag{19}$$

is the hyperbolic tangent mixing function approximation to the Heaviside step function. The parameter $\varsigma = z - z_b$, where z_b is the bottom depth, and L is the mixing length of this smoothing function.

Now, since $\tilde{n}^2 = n^2 + \frac{1}{2k_0^2}\left[\frac{1}{\rho}\frac{\partial^2 \rho}{\partial z^2} - \frac{3}{2}\left(\frac{1}{\rho}\frac{\partial \rho}{\partial z}\right)^2\right]$, we need to define

$$\frac{\partial \rho}{\partial z} = (\rho_b - \rho_w)\frac{\partial \bar{H}}{\partial z} = \frac{(\rho_b - \rho_w)}{4L}\operatorname{sech}^2\left(\frac{\varsigma}{2L}\right) \tag{20}$$

and

$$\frac{\partial^2 \rho}{\partial z^2} = (\rho_b - \rho_w)\frac{\partial^2 \bar{H}}{\partial z^2} = -\frac{(\rho_b - \rho_w)}{4L^2}\tanh\left(\frac{\varsigma}{2L}\right)\operatorname{sech}^2\left(\frac{\varsigma}{2L}\right). \tag{21}$$

Previous analysis by others [7], [9], [11], [12] has shown that good solutions result by choosing a mixing length of $L = \frac{2}{k_0} \approx \frac{\lambda}{\pi}$. Although this is an additional free parameter that could be evaluated for accuracy, we shall not explore this further in this thesis and will keep this mixing length defined throughout for those algorithms that utilize the density smoothing approach.

D. YEVICK AND THOMSON HYBRID IMPLEMENTATION TECHNIQUE

The hybrid approach by Yevick and Thomson [10] shows that the new formalism defining Q_1' requires evaluation of the additional operation

$$\Psi'(r + \Delta r, z) = \exp\left[i\delta\left(\sqrt{1+\gamma} - 1\right)\right]\tilde{\Psi}(r + \Delta r, z). \tag{22}$$

Note that this completes the range step if we only invoke the Q_1' approximation, and we may replace $\Psi' \to \Psi$. The Q_2' approximation requires an additional step and is discussed later.

Yevick and Thomson [10] proposed treatment of this operation through a finite difference approach, whereby the Pade approximation

$$\exp\left[i\delta\left(\sqrt{1+\gamma}-1\right)\right]\approx\frac{1+\frac{1}{4}(1+i\delta)\gamma}{1+\frac{1}{4}(1-i\delta)\gamma} \tag{23}$$

generates the finite difference equations

$$\left[1+\frac{1}{4}(1-i\delta)\gamma\right]\Psi(r+\Delta r,z)=\left[1+\frac{1}{4}(1+i\delta)\gamma\right]\tilde{\Psi}(r+\Delta r,z)\ . \tag{24}$$

In this case, direct application of γ is problematic since γ depends on $\frac{\partial\rho}{\partial z}$, and we do not want to invoke the smoothing function for ρ. Yevick and Thomson [10] show that an alternative is to evaluate a finite difference approximation to the original transverse operator

$$\mu'=\frac{\rho}{k_0^2}\frac{\partial}{\partial z}\left(\frac{1}{\rho}\frac{\partial}{\partial z}\right). \tag{25}$$

Then $\gamma=\mu'-\mu$, where μ is well-defined as an operator on Ψ.

Specifically, using a 3-point centered difference approximation defined by

$$f_0'\approx\frac{1}{h}\left(f_{\frac{1}{2}}-f_{-\frac{1}{2}}\right)+O\left(h^2\right), \tag{26}$$

then

$$\begin{aligned}\mu'\Psi=\frac{\rho}{k_0^2}\frac{\partial}{\partial z}\left(\frac{1}{\rho}\frac{\partial\Psi}{\partial z}\right)&\approx\frac{\rho}{\left(k_0\Delta z\right)^2}\left[\frac{1}{\rho_{\frac{1}{2}}}\left(\Psi_1-\Psi_0\right)-\frac{1}{\rho_{-\frac{1}{2}}}\left(\Psi_0-\Psi_{-1}\right)\right]\\&=\frac{\rho}{\left(k_0\Delta z\right)^2}\left[\frac{1}{\rho_{\frac{1}{2}}}\Psi_1-\left(\frac{1}{\rho_{\frac{1}{2}}}+\frac{1}{\rho_{-\frac{1}{2}}}\right)\Psi_0+\frac{1}{\rho_{-\frac{1}{2}}}\Psi_{-1}\right]\end{aligned} \tag{27}$$

where the indices $0,\ \pm\frac{1}{2},\ \pm1$ apply to the depth index in question and neighboring depths above and below.

Note that Yevick and Thomson assumed a continuous function for ρ, such that

$$\rho_{\frac{1}{2}} = \frac{1}{2}\left(\rho_1 + \rho_0\right) \ , \quad \rho_{-\frac{1}{2}} = \frac{1}{2}\left(\rho_0 + \rho_{-1}\right) \ . \tag{28}$$

However, we shall treat the density as defined by

$$\rho(z) = \rho_w + (\rho_b - \rho_w) H(z - z_b) = \begin{cases} \rho_w & , z < z_b; \\ \frac{1}{2}(\rho_w + \rho_b) & , z = z_b; \\ \rho_b & , z > z_b. \end{cases} \tag{29}$$

Then, since

$$\begin{aligned} \mu\Psi = \frac{1}{k_0^2}\frac{\partial^2}{\partial z^2}\Psi = \frac{1}{k_0^2}\frac{\partial}{\partial z}\left(\frac{\partial \Psi}{\partial z}\right) &\approx \frac{1}{k_0^2 \Delta z}\left[\left(\frac{\partial \Psi}{\partial z}\right)_{\frac{1}{2}} - \left(\frac{\partial \Psi}{\partial z}\right)_{-\frac{1}{2}}\right] \\ &\approx \frac{1}{\left(k_0 \Delta z\right)^2}\left[\left(\Psi_1 - \Psi_0\right) - \left(\Psi_0 - \Psi_{-1}\right)\right] = \frac{1}{\left(k_0 \Delta z\right)^2}\left[\Psi_1 - 2\Psi_0 + \Psi_{-1}\right] \end{aligned} \ , \tag{30}$$

we obtain

$$\gamma\Psi = \left(\mu' - \mu\right)\Psi = \frac{1}{\left(k_0 \Delta z\right)^2}\left[\left(\frac{\rho_0}{\rho_{\frac{1}{2}}} - 1\right)\Psi_1 - \left(\frac{\rho_0}{\rho_{\frac{1}{2}}} + \frac{\rho_0}{\rho_{-\frac{1}{2}}} - 2\right)\Psi_0 + \left(\frac{\rho_0}{\rho_{-\frac{1}{2}}} - 1\right)\Psi_{-1}\right]. \tag{31}$$

This agrees with Yevick and Thomson when their notation is employed, defined as

$$\begin{aligned} \frac{\rho_0}{\rho_{\frac{1}{2}}} &= \frac{\rho_0}{\frac{1}{2}\left(\rho_1 + \rho_0\right)} \equiv \rho_+ \\ \frac{\rho_0}{\rho_{-\frac{1}{2}}} &= \frac{\rho_0}{\frac{1}{2}\left(\rho_0 + \rho_{-1}\right)} \equiv \rho_- \\ \frac{\rho_0}{\rho_{\frac{1}{2}}} + \frac{\rho_0}{\rho_{-\frac{1}{2}}} &= 2\rho_0\left[\frac{1}{\left(\rho_1 + \rho_0\right)} + \frac{1}{\left(\rho_0 + \rho_{-1}\right)}\right] \equiv \rho_+ + \rho_- \ . \end{aligned} \tag{32}$$

For our discontinuous density, only integer index values of ρ have any meaning. So we shall define the notation $\rho_0 = \rho(z_0)$, $\rho_{\frac{1}{2}} \equiv \rho_+ = \rho(z > z_0)$, and $\rho_{-\frac{1}{2}} \equiv \rho_- = \rho(z < z_0)$. Then,

$$\gamma\Psi = \frac{1}{(k_0 \Delta z)^2}\left[\left(\frac{\rho_0}{\rho_+} - 1\right)\Psi_1 - \left(\frac{\rho_0}{\rho_+} + \frac{\rho_0}{\rho_-} - 2\right)\Psi_0 + \left(\frac{\rho_0}{\rho_-} - 1\right)\Psi_{-1}\right]. \tag{33}$$

We can then use a tridiagonal matrix solution to the expression

$$\underline{A}\bar{\Psi} = \underline{B}\tilde{\bar{\Psi}}, \tag{34}$$

where $\underline{A}$ has elements defined by $\left[1 + \frac{1}{4}(1 - i\delta)\gamma\right]$ and $\underline{B}$ has elements defined by $\left[1 + \frac{1}{4}(1 - i\delta)\gamma\right]$. Note that $\underline{A}$ and $\underline{B}$ are just identity matrices except in the vicinity of $z \sim z_b$, where γ is non-zero.

If we are only interested in the correction from the definition of Q_1', the solution is complete. However, Yevick and Thomson also go on to describe how this can be further refined through application of another finite difference approximation to the additional term in Q_2', i.e., $\exp\left\{-\frac{i\delta}{8}\left[\varepsilon(\mu + \gamma) + (\mu + \gamma)\varepsilon + \mu\gamma + \gamma\mu\right]\right\}$. Since $\mu + \gamma = \mu'$, we may write this as

$$\exp\left\{-\frac{i\delta}{8}\left[\varepsilon\mu' + \mu'\varepsilon + \mu\gamma + \gamma\mu\right]\right\} \approx \frac{1 - \frac{1}{16}i\delta(\varepsilon\mu' + \mu'\varepsilon + \mu\gamma + \gamma\mu)}{1 + \frac{1}{16}i\delta(\varepsilon\mu' + \mu'\varepsilon + \mu\gamma + \gamma\mu)}. \tag{35}$$

Note that for $\gamma = 0$, this correction simplifies to

$$\exp\left\{-\frac{i\delta}{8}(\varepsilon\mu + \mu\varepsilon)\right\} \approx \frac{1 - \frac{1}{16}i\delta(\varepsilon\mu + \mu\varepsilon)}{1 + \frac{1}{16}i\delta(\varepsilon\mu + \mu\varepsilon)}, \tag{36}$$

which can be applied as a correction to the existing MMPE approach based on $\tilde{Q}_2$ if we replace $\varepsilon \to \tilde{\varepsilon}$.

Yevick and Thomson drop the $\mu\gamma$ and $\gamma\mu$ terms, arguing that these are small, higher-order corrections, and instead utilize the correction [10]

$$\exp\left[-\frac{i\delta}{8}\left(\varepsilon\mu' + \mu'\varepsilon\right)\right] \approx \frac{1-\frac{1}{16}i\delta\left(\varepsilon\mu' + \mu'\varepsilon\right)}{1+\frac{1}{16}i\delta\left(\varepsilon\mu' + \mu'\varepsilon\right)} \ . \tag{37}$$

This produces the additional correction for

$$\Psi\left(r+\Delta r, z\right) = \exp\left[-\frac{i\delta}{8}\left(\varepsilon\mu' + \mu'\varepsilon\right)\right]\Psi'\left(r+\Delta r, z\right) \tag{38}$$

where we again invoke the matrix approach

$$\underline{A}\vec{\Psi} = \underline{B}\vec{\Psi}', \tag{39}$$

and elements of $\underline{A}$ are defined by $1+\frac{1}{16}i\delta\left(\varepsilon\mu' + \mu'\varepsilon\right)$ while the elements of $\underline{B}$ are defined by $1-\frac{1}{16}i\delta\left(\varepsilon\mu' + \mu'\varepsilon\right)$.

The evaluation of $\varepsilon\mu'\Psi$ follows Eq. (27),

$$\varepsilon\mu'\Psi \approx \frac{\varepsilon_0\rho_0}{\left(k_0\Delta z\right)^2}\left[\frac{1}{\rho_{\frac{1}{2}}}\Psi_1 - \left(\frac{1}{\rho_{\frac{1}{2}}} + \frac{1}{\rho_{-\frac{1}{2}}}\right)\Psi_0 + \frac{1}{\rho_{-\frac{1}{2}}}\Psi_{-1}\right] . \tag{40}$$

However, for $\mu'\varepsilon\Psi$ we must consider

$$\mu'(\varepsilon\Psi) = \frac{\rho_0}{k_0^2}\frac{\partial}{\partial z}\left[\frac{1}{\rho}\frac{\partial(\varepsilon\Psi)}{\partial z}\right] \approx \frac{\rho_0}{k_0^2\Delta z}\frac{\partial}{\partial z}\left[\frac{1}{\rho}\left(\varepsilon_{\frac{1}{2}}\Psi_{\frac{1}{2}} - \varepsilon_{-\frac{1}{2}}\Psi_{-\frac{1}{2}}\right)\right]$$

$$= \frac{\rho_0}{(k_0\Delta z)^2}\left[\frac{1}{\rho_{\frac{1}{2}}}(\varepsilon_1\Psi_1 - \varepsilon_0\Psi_0) - \frac{1}{\rho_{-\frac{1}{2}}}(\varepsilon_0\Psi_0 - \varepsilon_{-1}\Psi_{-1})\right] \tag{41}$$

$$= \frac{\rho_0}{(k_0\Delta z)^2}\left[\frac{1}{\rho_{\frac{1}{2}}}\varepsilon_1\Psi_1 - \left(\frac{1}{\rho_{\frac{1}{2}}} + \frac{1}{\rho_{-\frac{1}{2}}}\right)\varepsilon_0\Psi_0 + \frac{1}{\rho_{-\frac{1}{2}}}\varepsilon_{-1}\Psi_{-1}\right] .$$

Note that if we are applying only this correction to MMPE, then the correction would result from the application of Equation (36) to $\underline{A}\tilde{\Psi}(r+\Delta r, z) = \underline{B}\tilde{\Psi}'(r+\Delta r, z)$. Here,

$$\varepsilon\mu\Psi \approx \frac{\varepsilon_0}{(k_0\Delta z)^2}\left[\Psi_1 - 2\Psi_0 + \Psi_{-1}\right] \tag{42}$$

and

$$\mu\varepsilon\Psi \approx \frac{1}{(k_0\Delta z)^2}\left[\varepsilon_1\Psi_1 - 2\varepsilon_0\Psi_0 + \varepsilon_{-1}\Psi_{-1}\right] . \tag{43}$$

As before, we would need to replace $\varepsilon \to \tilde{\varepsilon}$ if we are utilizing the density smoothing approach.

E. TAPPERT SMOOTHING FUNCTION APPROACH

In 1991, Tappert [13] suggested an alternative to the effective index term in the smoothing function as

$$\tilde{n}^2 = n^2 - \frac{\alpha}{k_0^2}\frac{\partial^2\bar{H}(\varsigma)}{\partial z^2} \quad , \quad \alpha = \frac{1-(\rho_w/\rho_b)^{\frac{1}{2}}}{1+(\rho_w/\rho_b)^{\frac{1}{2}}} \quad . \tag{44}$$

This method can utilize the existing MMPE code by simply replacing the effective index of refraction term with Equation (44). We shall utilize the same definition for the mixing

length, $L = \frac{2}{k_0}$, although Tappert believed this should improve the model as both Δz and L get smaller. We shall not investigate the effect of reducing the mixing length with this approach further in this thesis.

THIS PAGE INTENTIONALLY LEFT BLANK

III. RESULTS

A. MMPE USER INTERFACE

The MMPE input parameters give the user the ability to manually define the grid size. This is accomplished by changing the "pefiles.inp" input file in the local directory. The depth grid size is defined indirectly by changing *nz* in "pefiles.inp" to the desired length of the FFT size to be used in the calculation. This value determines the number of depth samples at each range step according to $\Delta z = 2z_{\max}/nz$, where $z_{\max}$ is the maximum computational depth. The factor 2 accounts for the image solution method employed in SSF algorithms. Similarly, the range step size can be manually defined by changing *rfact*. This defines the range step by multiplying Δz by *rfact*. Therefore, an *rfact* = 1 makes a uniform grid in which the depth grid size and the range step size are equal. An *rfact* >1 makes the range step size larger than the depth grid size (and vice versa). If Δz and *rfact* are set to 0.0, the model will automatically define $\Delta z = \lambda/10$ and $\Delta r = \lambda$, where λ is the acoustic wavelength be computed.

B. NO DENSITY CASE

The original MMPE and both alternate options were used to model the transmission loss in an ocean environment with no density discontinuity at the bottom interface. In each case, the MMPE model was allowed to automatically determine the grid size based on the default values of Δz and Δr, i.e., $\Delta z = \lambda/10$ and $\Delta r = \lambda$. The solution for the alternate implementation methods were confirmed to be identical to the solution obtained in the original MMPE model, since there is no density discontinuity calculation in this example. All solutions closely match the benchmark solution, as observed in Figure 2.

Since both alternate implementation options exactly match the original MMPE solution in this environment, only the original MMPE model was used to find the optimum Δr in the case without a density contrast. The Δr variability study was conducted by varying *rfact* while holding *nz* constant.

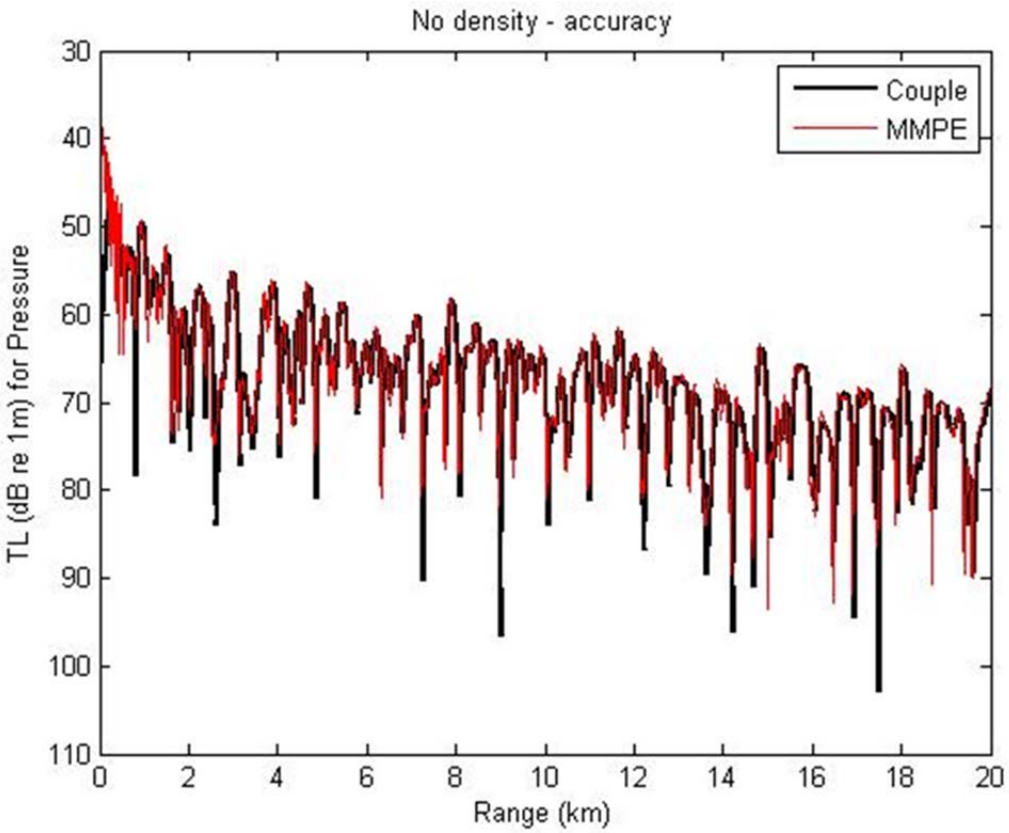

Figure 2. Original MMPE vs. Couple, no density discontinuity.

a. Results for nz = 512

Figures 3–6 show the results for a fixed value of *nz* = 512, corresponding to a Δz of approximately 5 m, or $\Delta z \approx \lambda/3$, with *rfact* values of 50, 20, 10, 5, 1, 0.2, 0.1, and 0.05. These graphs show two notable features: that the model converges to a stable solution and that the stable solution tends to underestimate the transmission loss of the benchmark solution and lacks structure. Focusing on the transmission loss from 15–20 km, as depicted in Figure 7, allows us to better see the model's convergence. For the *nz* = 512 case, the solution tends to converge at *rfact* values smaller than 1.

Since an *rfact* = 5 overestimated transmission loss when compared with the benchmark solution, and *rfact* = 1 underestimated the transmission loss, there must be an optimum *rfact* between these values which provides the most accurate solution when

compared to the benchmark. The optimum value for the *nz* = 512 case is determined to be 2.5, as shown in Figure 8. This corresponds to a Δr of approximately 12 m, or $\Delta r \sim \lambda$.

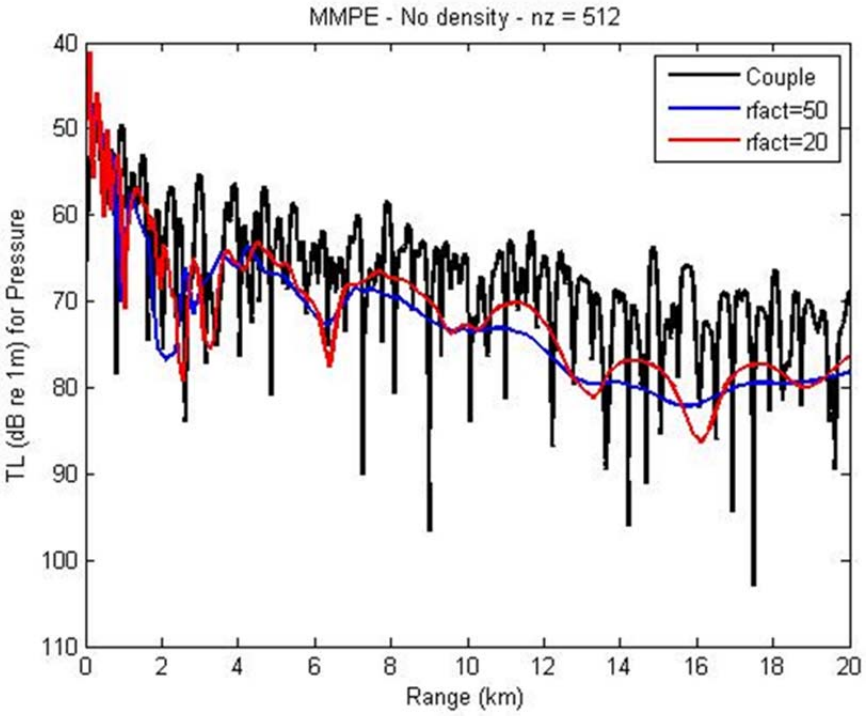

Figure 3. Original MMPE, no density, *nz* = 512, *rfact* = 50, 20.

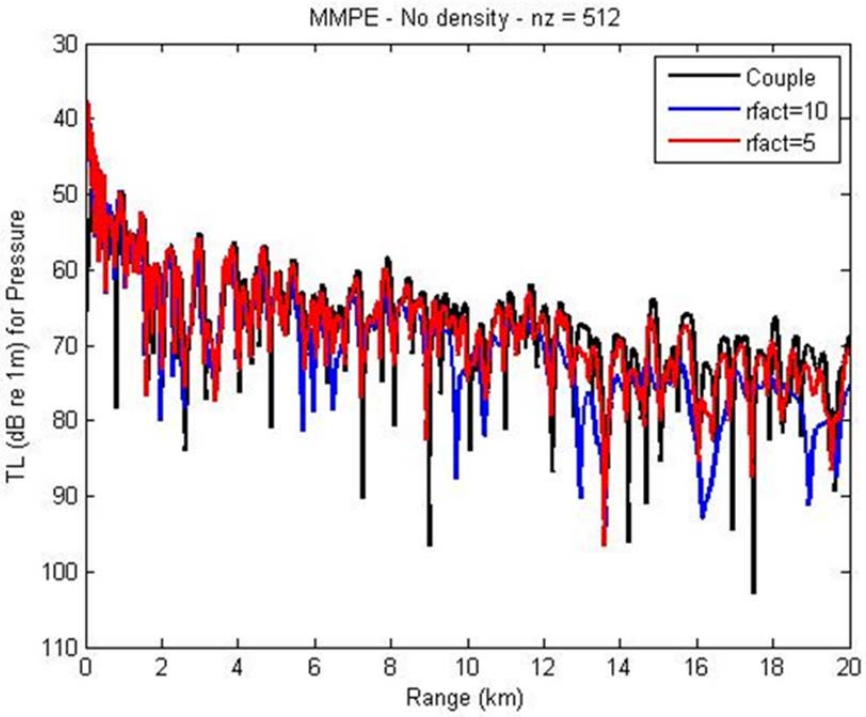

Figure 4. Original MMPE, no density, *nz* = 512, *rfact* = 50, 20.

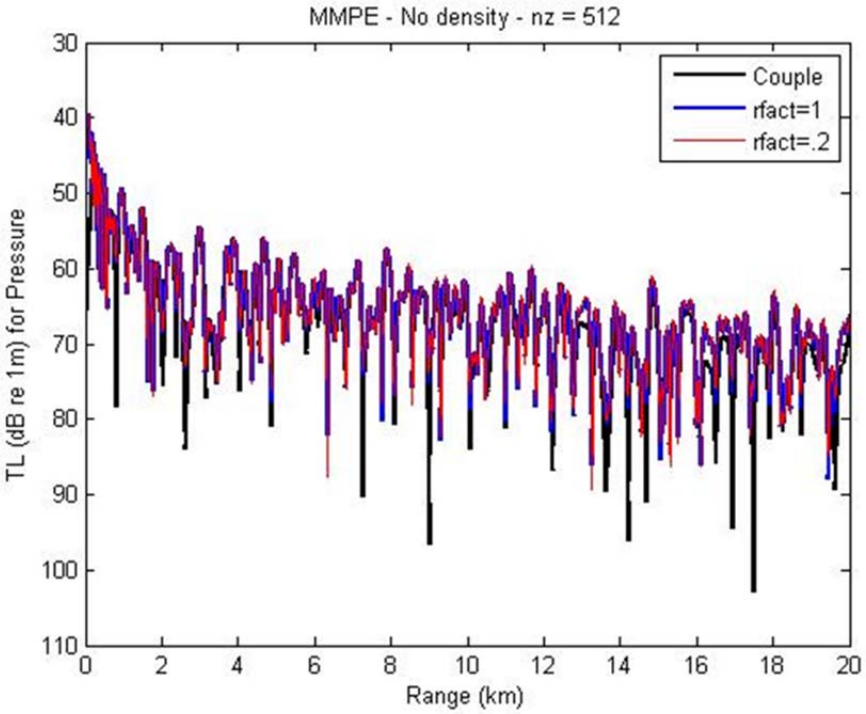

Figure 5. Original MMPE, no density, *nz* = 512, *rfact* = 1, 0.2.

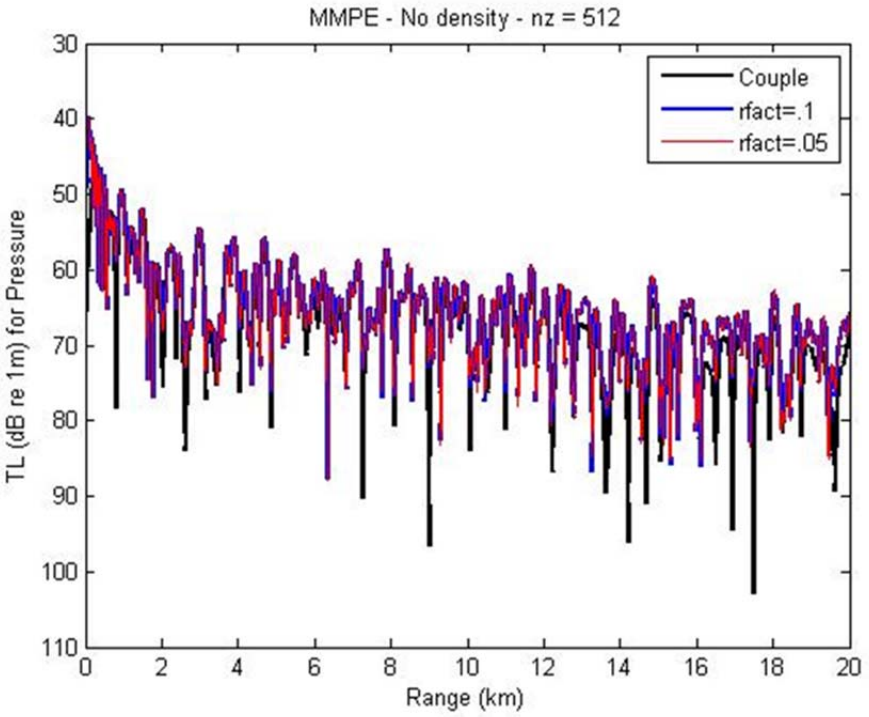

Figure 6. Original MMPE, no density, *nz* = 512, *rfact* = 0.1, 0.05.

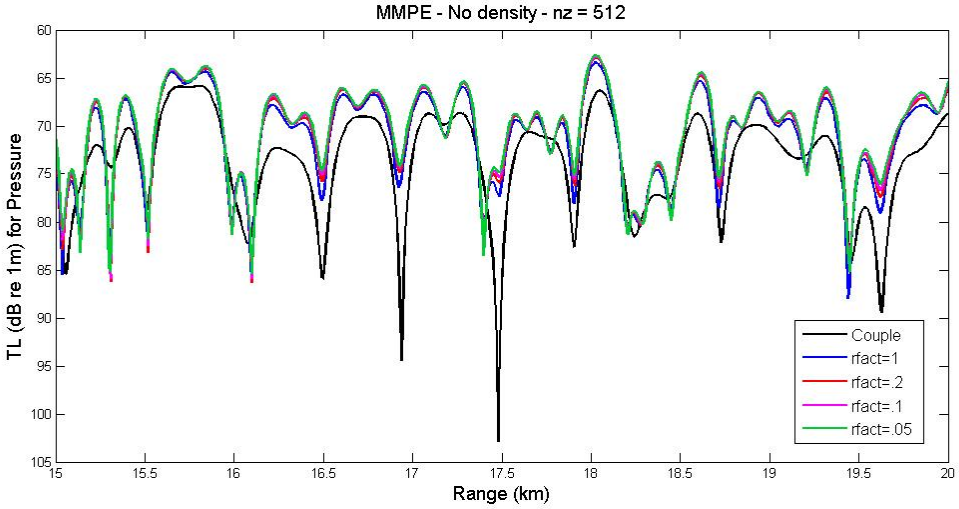

Figure 7. Solution convergence for *nz* = 512.

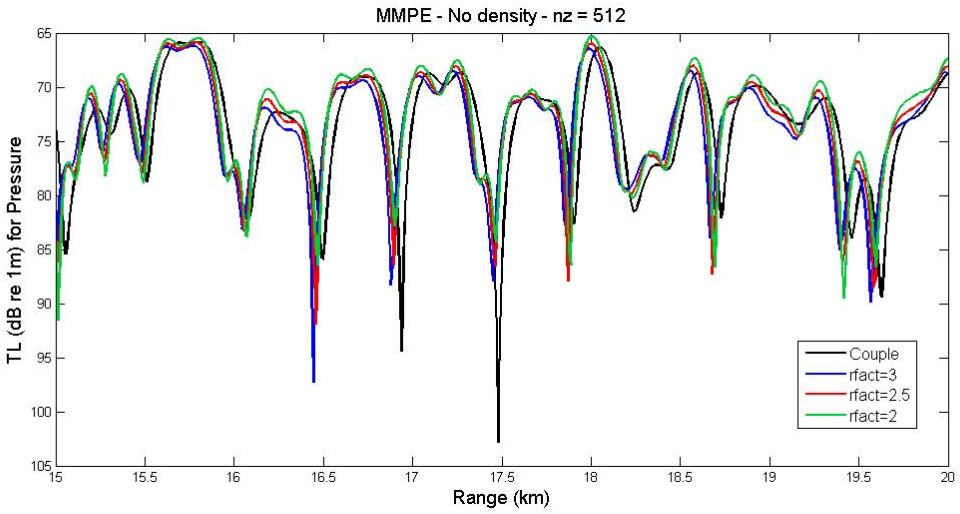

Figure 8. Closest approximation to benchmark solution, *nz* = 512.

b. Results for nz = 1024

The process was repeated as Δz was decreased with similar results. Here, the depth mesh is approximately 10 m, or $\Delta z \sim \lambda/6$. The solution again converges at a value that slightly underestimates transmission loss as observed in Figures 9–13. In this case, the optimum *rfact* is determined to be 5 as shown in Figure 14. This again corresponds to a Δr of approximately 12 m, or $\Delta r \sim \lambda$.

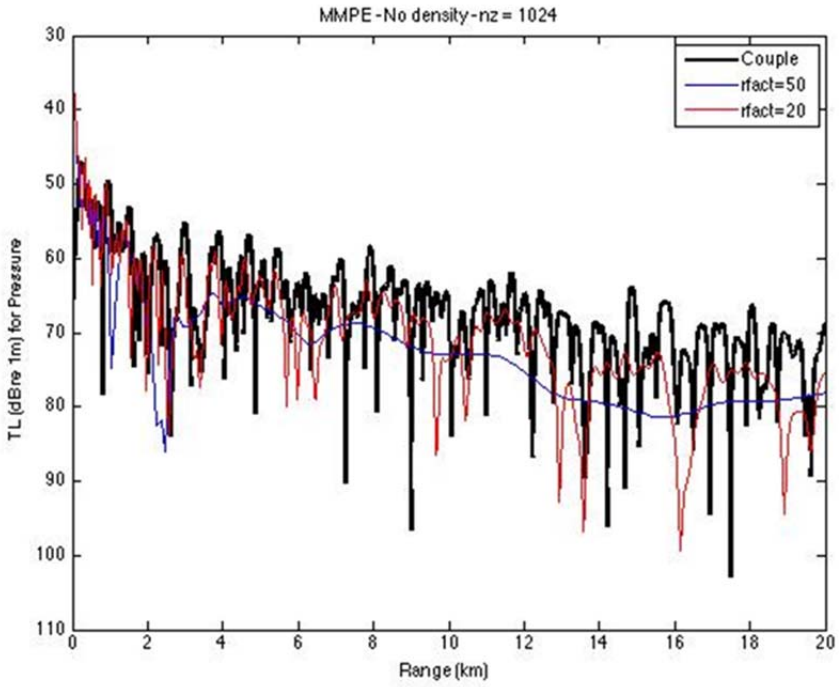

Figure 9. Original MMPE, no density, *nz* = 1024, *rfact* = 50, 20.

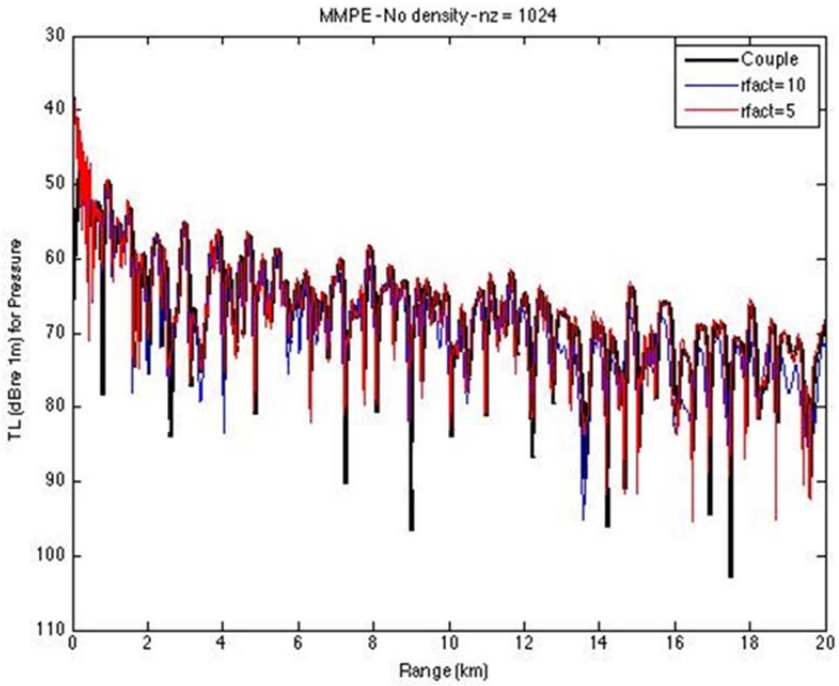

Figure 10. Original MMPE, no density, *nz* = 1024, *rfact* = 10, 5.

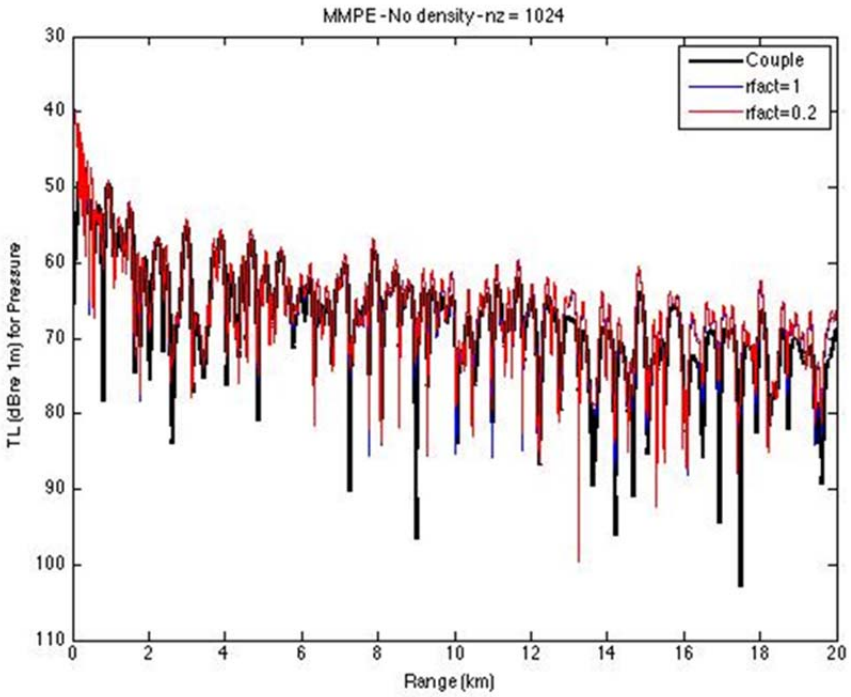

Figure 11. Original MMPE, no density, *nz* = 1024, *rfact* = 1, 0.2.

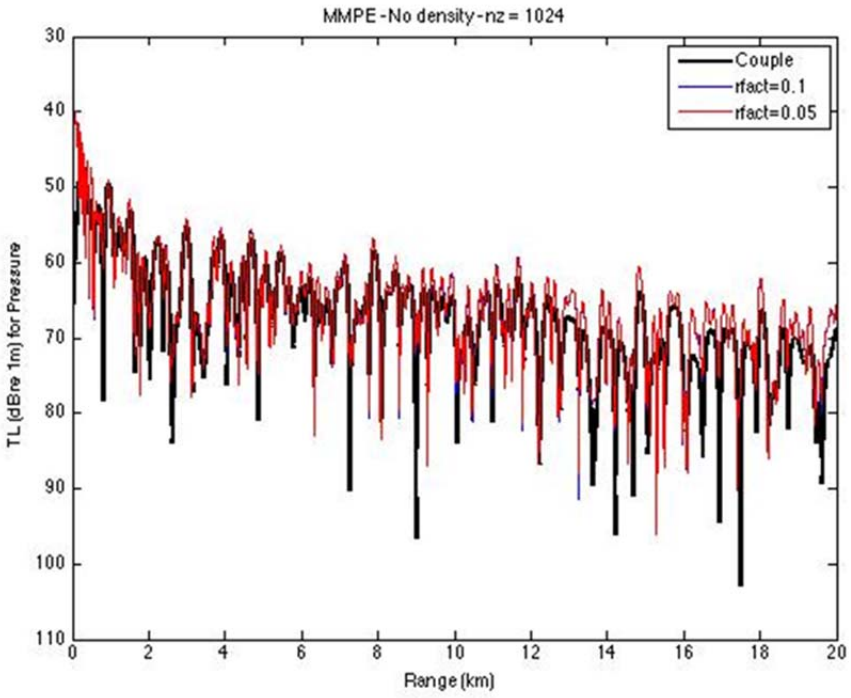

Figure 12. Original MMPE, no density, *nz* = 1024, *rfact* = 0.1, 0.05.

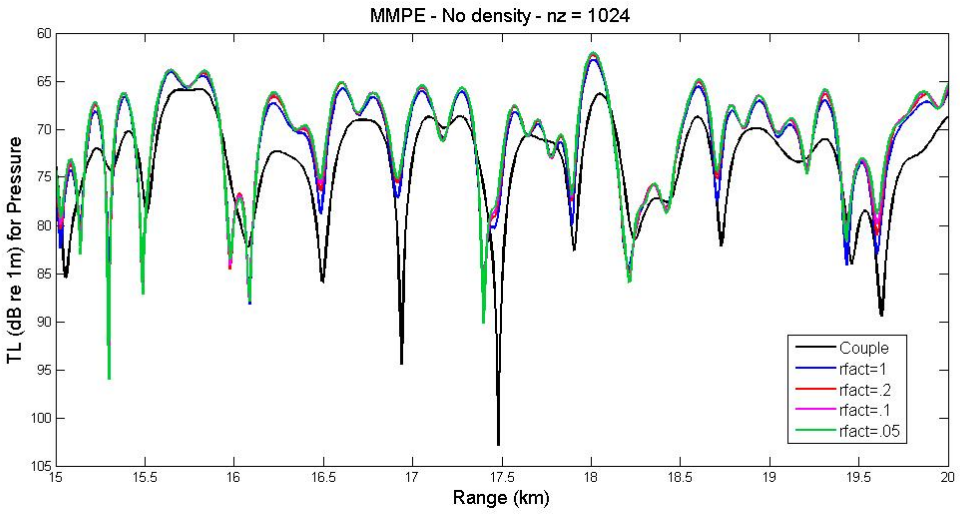

Figure 13. Solution convergence for *nz* = 1024.

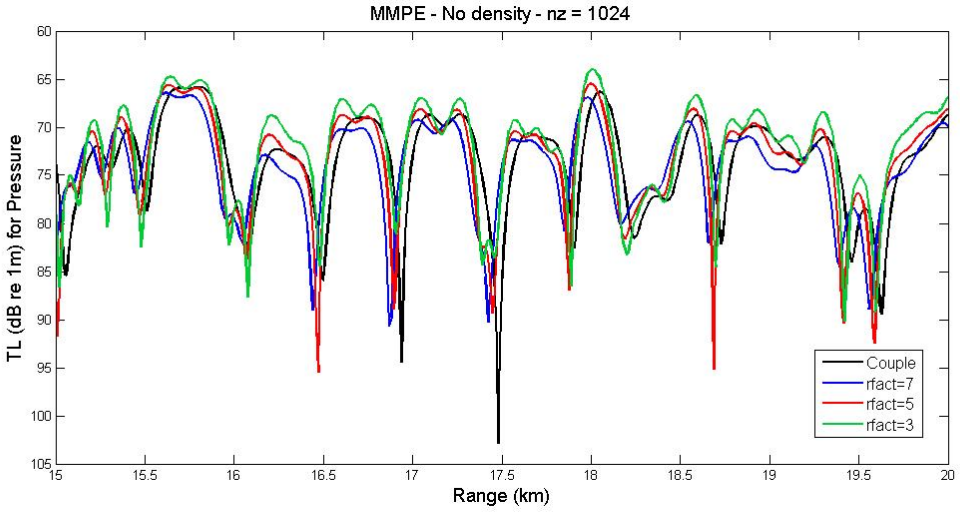

Figure 14. Closest approximation to benchmark solution, *nz* = 1024.

c. Results for nz>1024

The model was also evaluated at *nz* values of 2048, 4096, 8192, and 16,384. The results for smaller Δz were similar to those obtained for *nz* = 512 and 1024. In all cases, the solution converges at a value slightly lower than the benchmark solution and the optimum solution occurs when Δr is approximately 12 m, or $\Delta r \sim \lambda$. See the Appendix for full results.

C. MODEL RESULTS IN PRESENCE OF DENSITY DISCONTINUITY

All three implementation options for the MMPE model were employed in an environment with a density contrast at the bottom interface. The range step size was held constant at 12 m while the depth grid size was reduced for each implementation method. Range step correction factors slightly higher and lower were also tested against a varying depth grid size.

1. Original MMPE

With a fixed Δr=12 m, there are negligible differences in the transmission loss model as observed in Figure 15. In this case, an *nz* value of 512 is not only the most efficient calculation, but also provides a transmission loss solution that is not significantly different than those obtained from a finer depth grid. As noted, for $nz = 512$, the depth mesh is approximately $\Delta z \approx 5\,\text{m} \sim \lambda/3$.

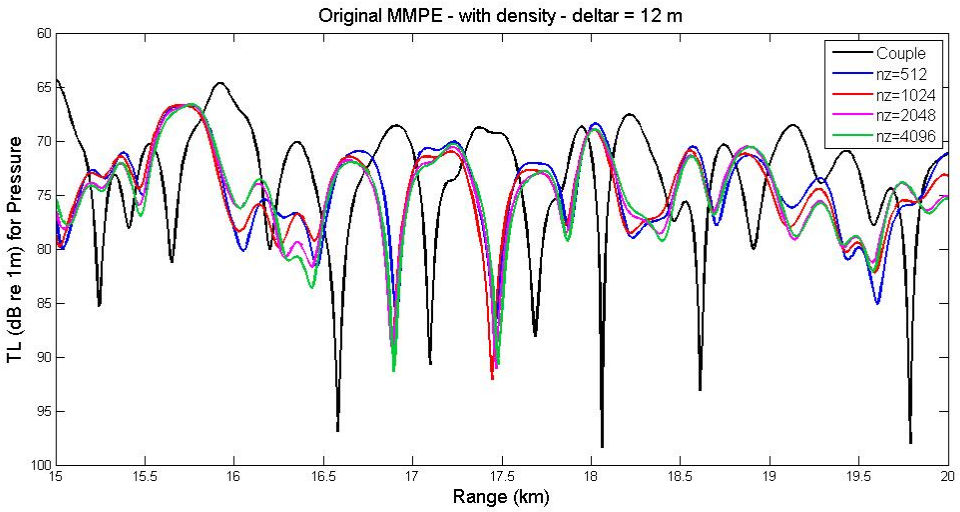

Figure 15. Original MMPE, Δr = 12 m, various *nz*.

2. MMPE with Tappert Smoothing Function

Figure 16 shows similar results when the Tappert smoothing function is implemented into the MMPE model. When compared to the original MMPE, the differences in the model are even less significant as Δz is decreased.

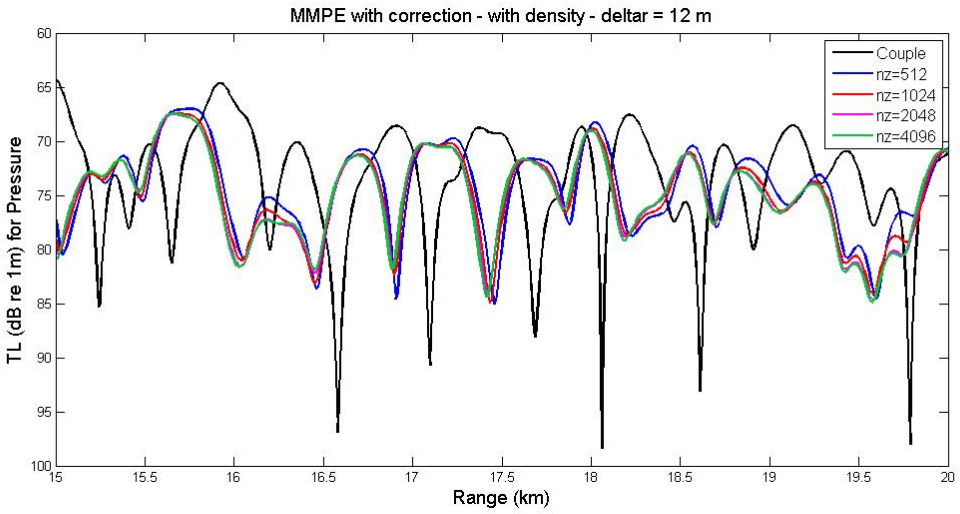

Figure 16. MMPE with Tappert smoothing function, $\Delta r = 12$ m, various *nz*.

3. Yevick and Thomson Hybrid Implementation

Yevick and Thomson's SSF/FD hybrid implementation provides for some interesting results. At the largest Δz (*nz* = 512), the model is a poor comparison to the benchmark solution at range. The solution underestimates the benchmark solution at all values. Furthermore the shape of the graph only vaguely represents the benchmark solution. Decreasing the depth grid size by a factor of 2 results in an even worse solution as seen in Figure 17. However, decreasing Δz beyond this point improved the solution dramatically. At *nz* = 2048, the solution begins approaching the benchmark solution, both in overall shape and magnitude of transmission loss. The hybrid model most closely approximates the benchmark solution at *nz* = 8192, corresponding to $\Delta z \approx 0.3 \text{ m} \sim \lambda/50$. Decreasing Δz further results in smaller changes to the solution as observed in Figure 18.

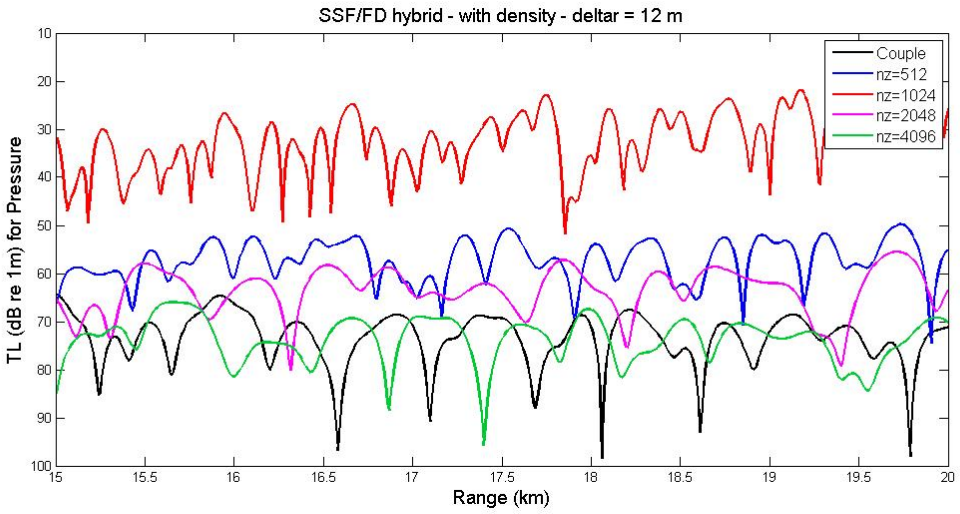

Figure 17. Hybrid implementation, $\Delta r = 12$ m, various *nz* (coarse Δz).

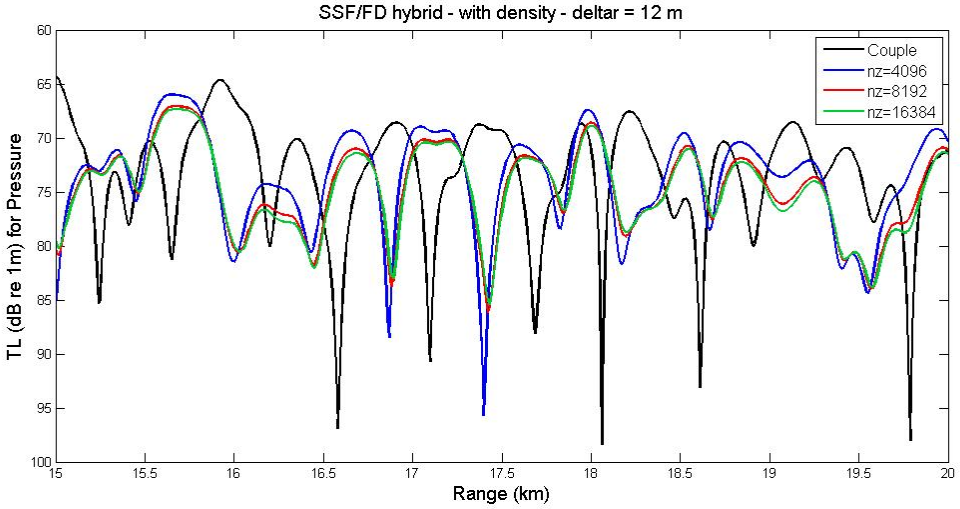

Figure 18. Hybrid implementation, $\Delta r = 12$ m, various *nz* (fine Δz).

4. Overall Comparison

Solutions for the original MMPE, MMPE with Tappert smoothing function, and Yevick and Thomson's hybrid implementation are compared in Figure 19. An *nz* value of 512 ($\Delta z \sim \lambda/3$) is used for both the original version of the MMPE model and the MMPE model with the Tappert alternative method, since that value was efficient and smaller Δz values did not significantly affect the solution accuracy. An *nz* value of 8192 ($\Delta z \sim \lambda/50$)

is used for the hybrid implementation option since that value provided for the most accurate solution for the hybrid implementation technique. The figure shows there is marginal difference between the original MMPE and MMPE with the Tappert alternative function. The hybrid implementation option provides for a slightly closer approximation to the benchmark solution in amplitude, however is a less efficient solution. In all cases, though, the phase error exists at this long range. Thus, it does not appear that this phase error is caused by inaccuracies in the computational treatment of the smoothing function, or the first order correction in the hybrid method defined in Equation (22).

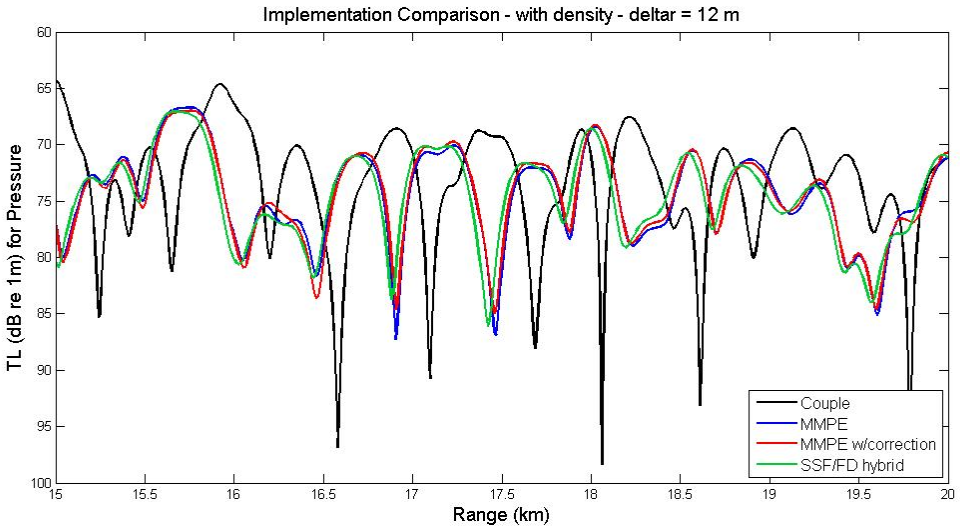

Figure 19. Implementation method comparison.

5. Effect of Reference Sound Speed

To this point, the reference sound speed for all transmission loss solutions was held constant at 1500 m/s. However, varying the reference sound speed has a significant effect on the phase of the solution. In general, the magnitudes of the solutions are unchanged, but the phase error present can be minimized. Figures 20–23 show the results when the reference sound speed is varied. The previously determined optimum depth mesh and range step is used for each implementation option. The best solution appears to occur at a reference sound speed of 1480 m/s. Figure 24 shows the results of all three implementation options at the optimum reference sound speed.

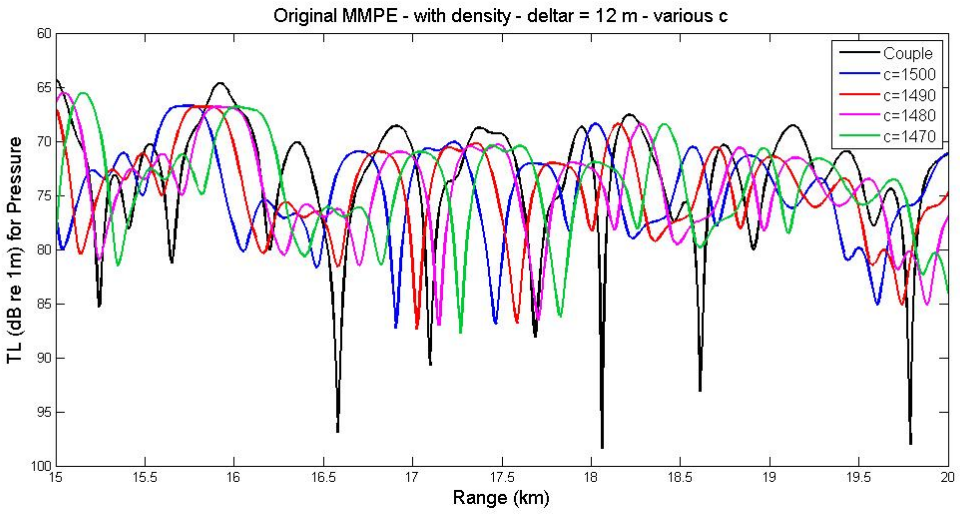

Figure 20. Original MMPE, Δr = 12 m, *nz* = 512, various c_0.

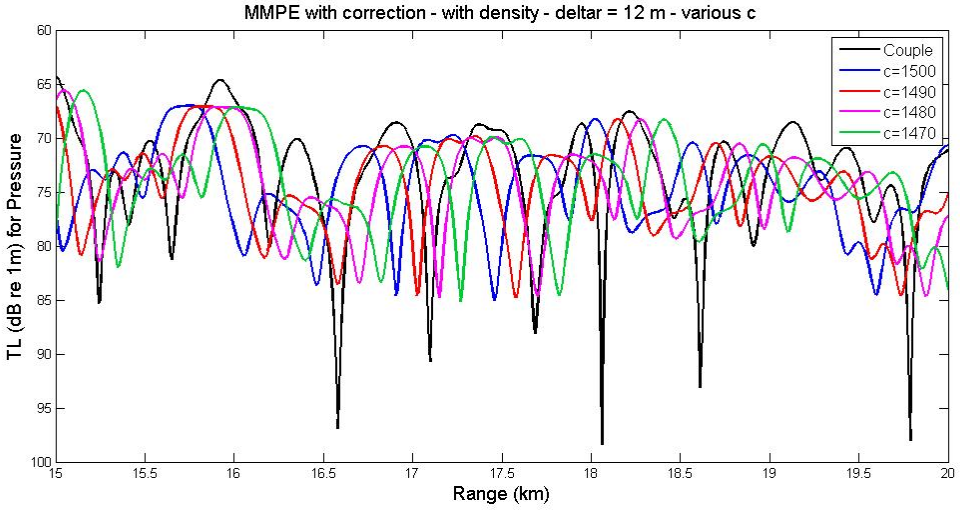

Figure 21. MMPE with Tappert smoothing, Δr = 12 m, *nz* = 512, various c_0.

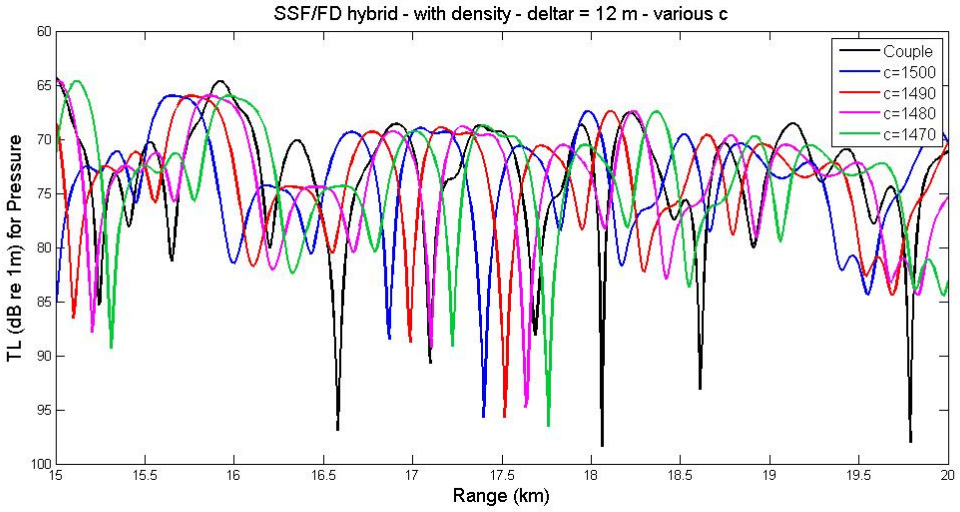

Figure 22. Hybrid implementation, Δr = 12 m, *nz* = 8192, various c_0.

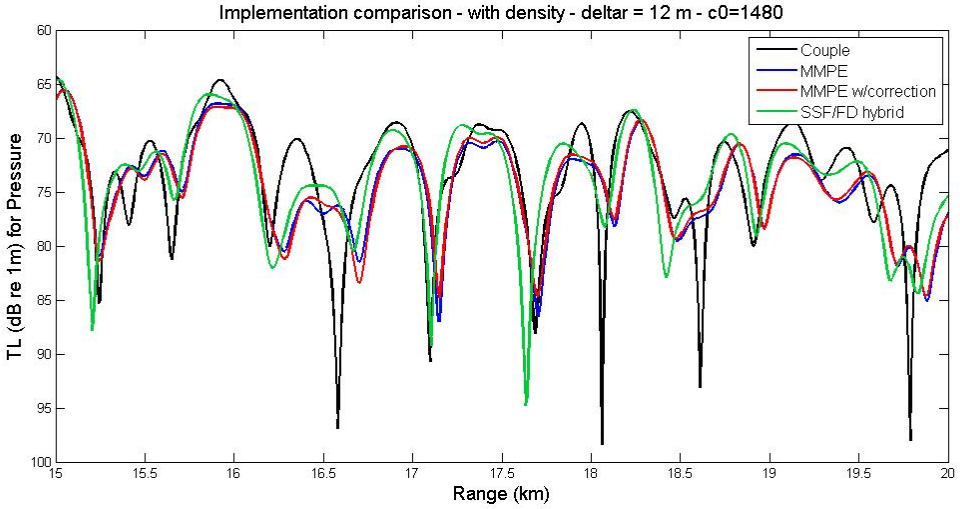

Figure 23. Implementation comparison, Δr = 12 m, 15–20 km.

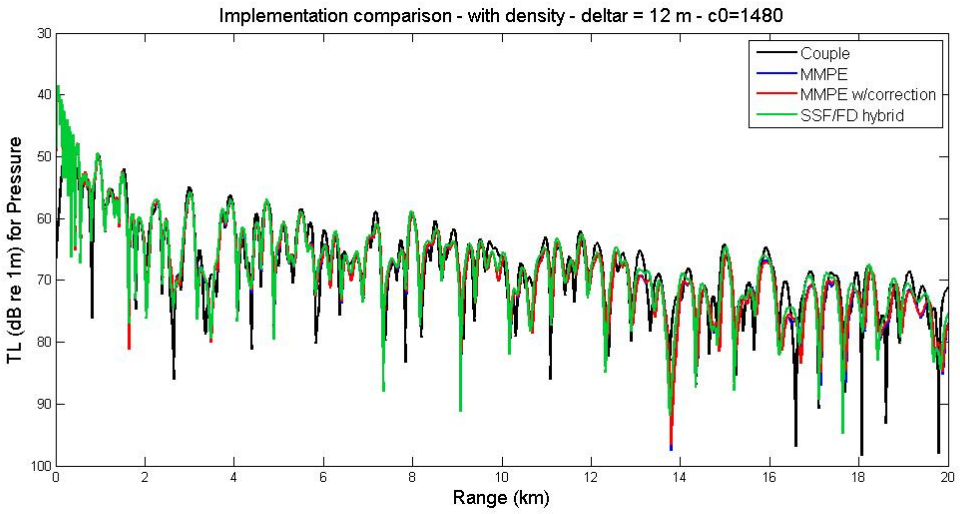

Figure 24. Implementation comparison, Δr = 12 m, 0–20 km.

The model's inaccuracies at range appear primarily due to the phase errors. Alternate implementation options did not significantly correct the phase error. Proper selection of reference sound speed seems to correct this error. This was previously noted in a deep water benchmark problem defined in the 1993 PE Workshop [12], and subsequent work by Tappert [13] using his "c_0-insensitive" version seemed to correct the phase errors. Yevick and Thomson [10] were also able to correct the phase error found in the deep water PE Workshop problem by implementing their higher-order correction term, defined in Equation (38), in their hybrid method. It is quite possible that implementation of that higher-order correction term would also address the phase error found in the shallow water problem defined in this thesis. Although not as efficient as a basic SSF method, the proposed hybrid method with higher-order correction might be expected to improve the long-range phase accuracy of all solutions.

IV. SUMMARY

The parabolic equation method for transmission loss modeling is an important topic in the acoustics scientific community. The SSF technique has been used for years due to its computational efficiency. Presently, SSF techniques provide accurate solutions in deep ocean environments where bottom interactions are negligible. However, as the focus shifts to shallow water acoustic propagation, it becomes necessary to find a way to use the SSF algorithm to model transmission loss. This paper compares two different implementation techniques when compared to a standard SSF model.

The basic SSF algorithm employing the Thomson-Chapman WAPE approximation employed in the MMPE model was found to be very accurate when there is no density discontinuity present. As the depth mesh grid is reduced in size, the MMPE model converges to a stable solution. When compared to the benchmark solution, the convergence in Δr slightly underestimates transmission loss at all ranges. This is presumably due to numerical noise when the range step becomes too small. By systematically reducing Δr it is shown that an optimal comparison exists at a $\Delta r \sim \lambda$. This optimal value for Δr remains constant even as Δz is decreased and a density discontinuity is introduced.

In the presence of a density discontinuity, both the original MMPE, and MMPE with the alternate Tappert approach to treating the effective index of refraction function, provide a fair model of the magnitude of transmission loss at ranges greater than 15 km. The largest tested Δz of approximately $\lambda/4$ provided acceptable results. Decreasing Δz further does not significantly change the solutions' accuracy. Since a smaller Δz results in increased computational time, it is recommended that a Δz of approximately $\lambda/4$ be used for both options.

The implementation of Yevick and Thomson's hybrid technique was able to provide a slightly more accurate comparison to the benchmark solution amplitude. However, it is necessary to make Δz very small in order to obtain such comparable

results. This comes at the cost of increased computational complexity, and should be balanced against the need to obtain the most accurate result.

All models were found to suffer from a phase error, which accumulates in range when a reference sound speed of 1500 m/s is used. This phase error can be minimized by lowering c_0 to 1480 m/s. This is reminiscent of previous phase errors found with the Thomson-Chapman WAPE approximation. It is quite possible that these phase errors may be significantly reduced by employing the higher-order correction of Yevick and Thomson, or the c_0-insensitive version of the SSF algorithm defined by Tappert. Future work could investigate the relative accuracy of each of these methods.

APPENDIX. MMPE CONVERGENCE GRAPHS

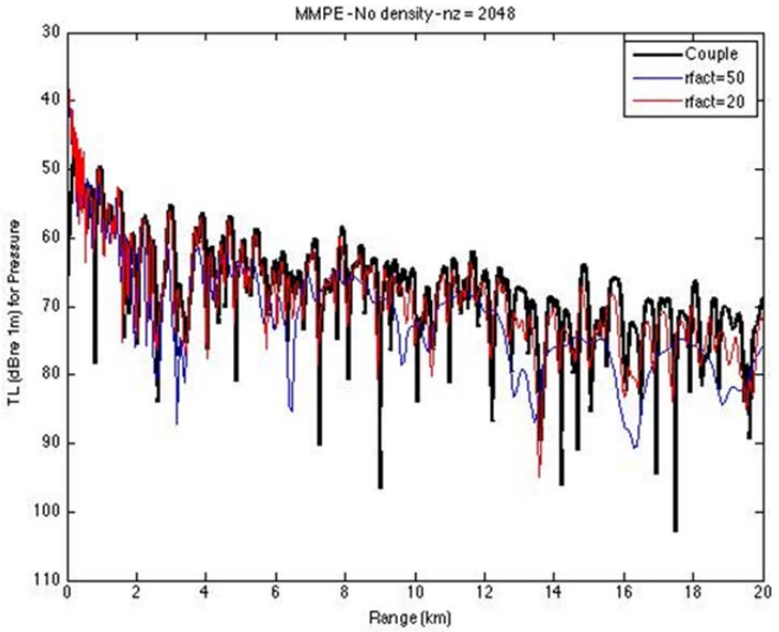

Figure 25. Original MMPE, no density, *nz* = 2048, *rfact* = 50, 20.

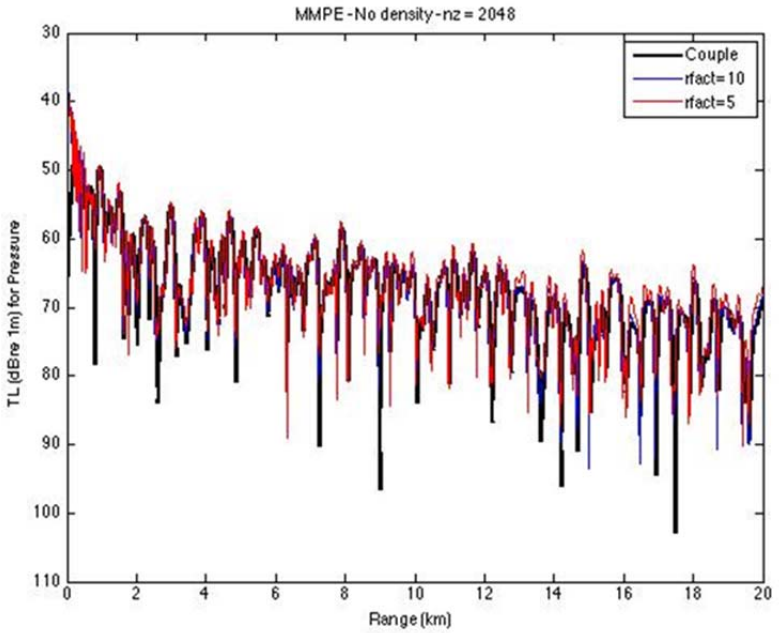

Figure 26. Original MMPE, no density, *nz* = 2048, *rfact* = 10, 5.

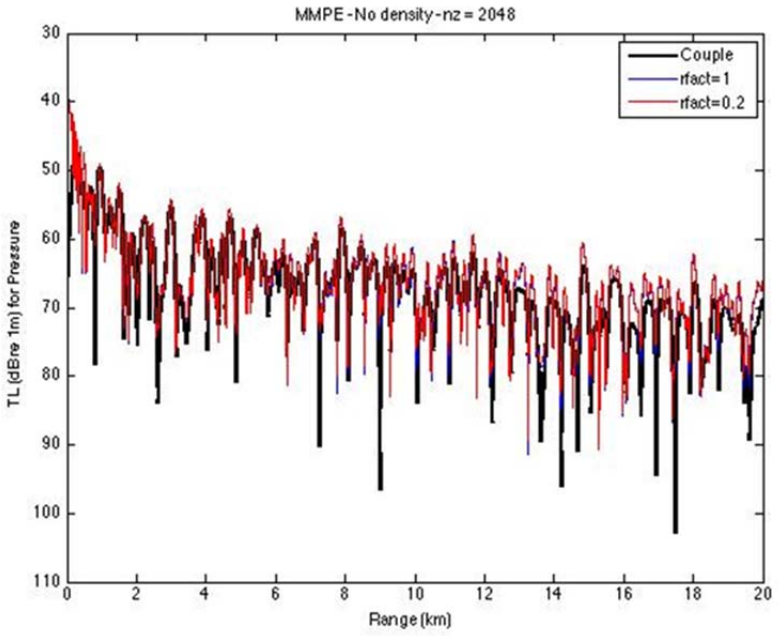

Figure 27. Original MMPE, no density, *nz* = 2048, *rfact* = 1, 0.2.

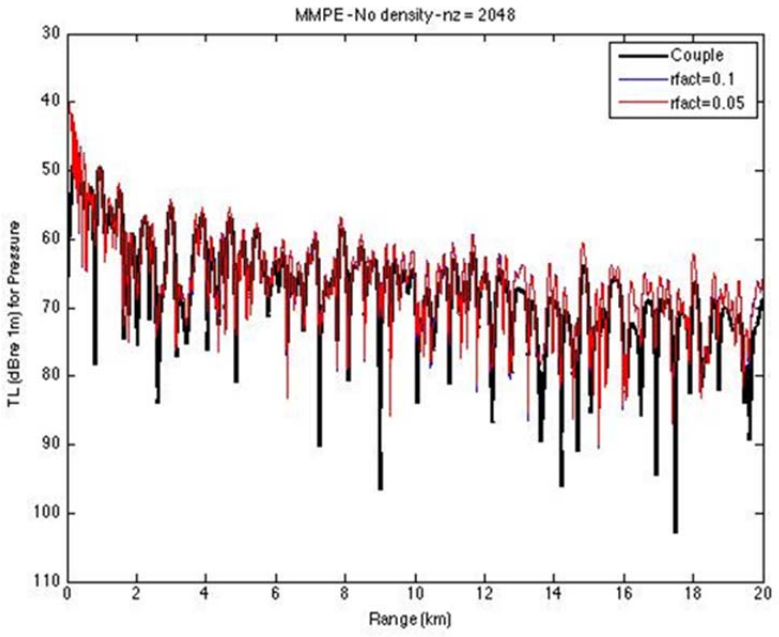

Figure 28. Original MMPE, no density, *nz* = 2048, *rfact* = 0.1, 0.05.

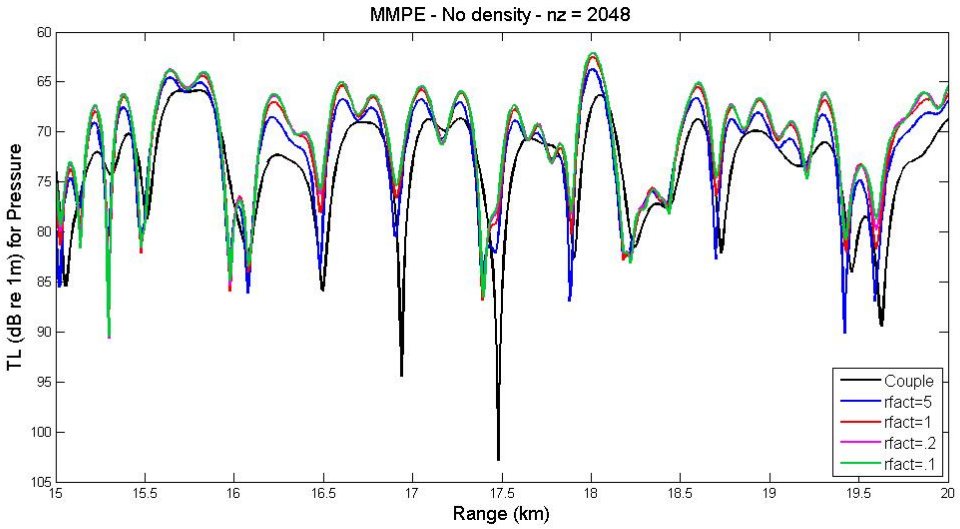

Figure 29. Solution convergence for *nz* = 2048.

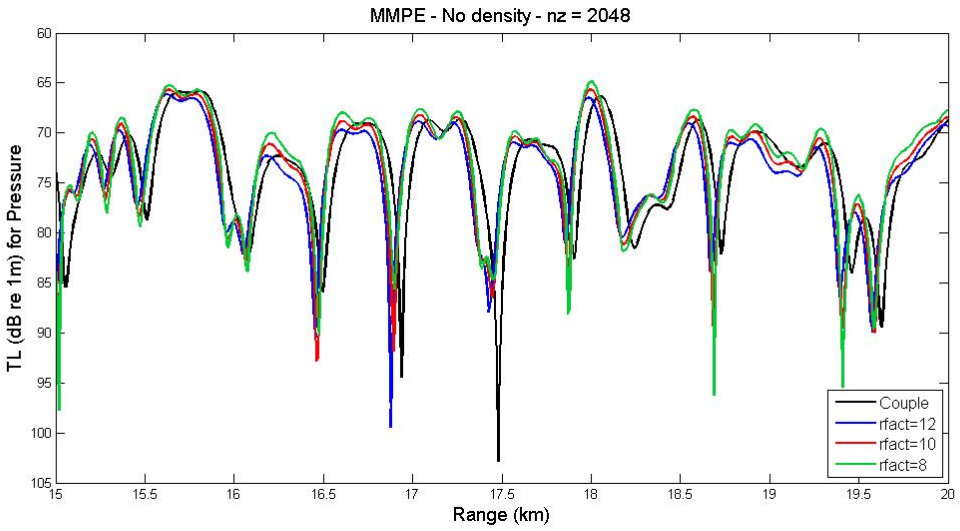

Figure 30. Closest approximation to benchmark solution, *nz* = 2048.

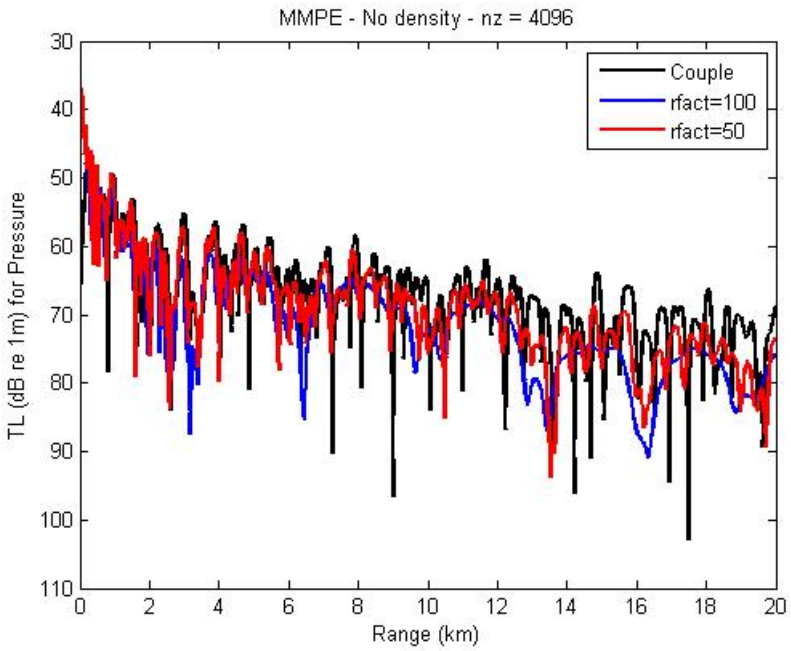

Figure 31. Original MMPE, no density, *nz* = 4096, *rfact* = 100, 50.

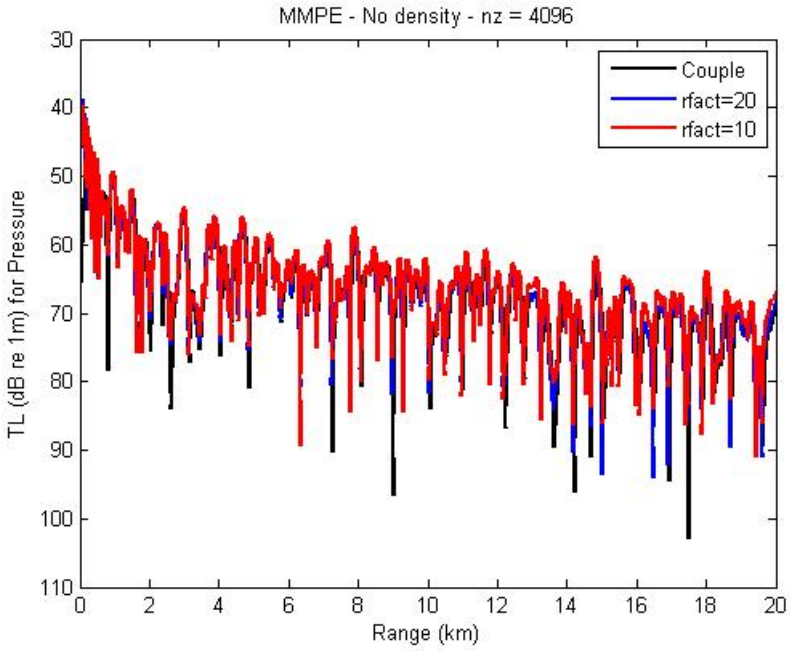

Figure 32. Original MMPE, no density, *nz* = 4096, *rfact* = 20, 10.

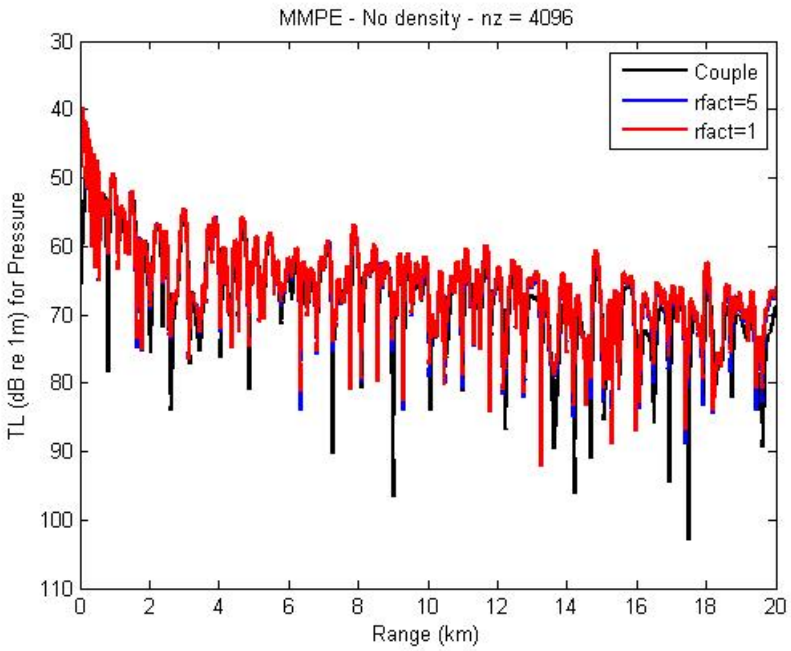

Figure 33. Original MMPE, no density, *nz* = 4096, *rfact* = 5, 1.

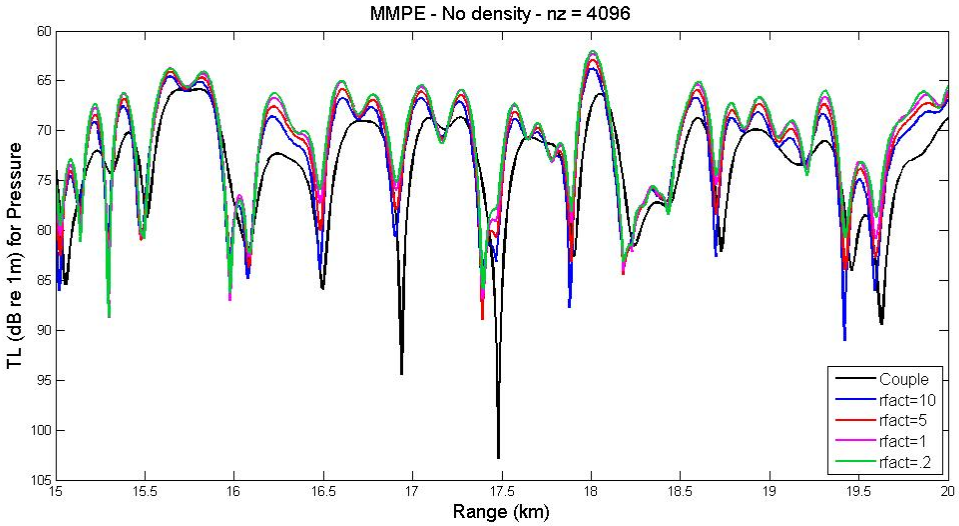

Figure 34. Solution convergence for *nz* = 4096.

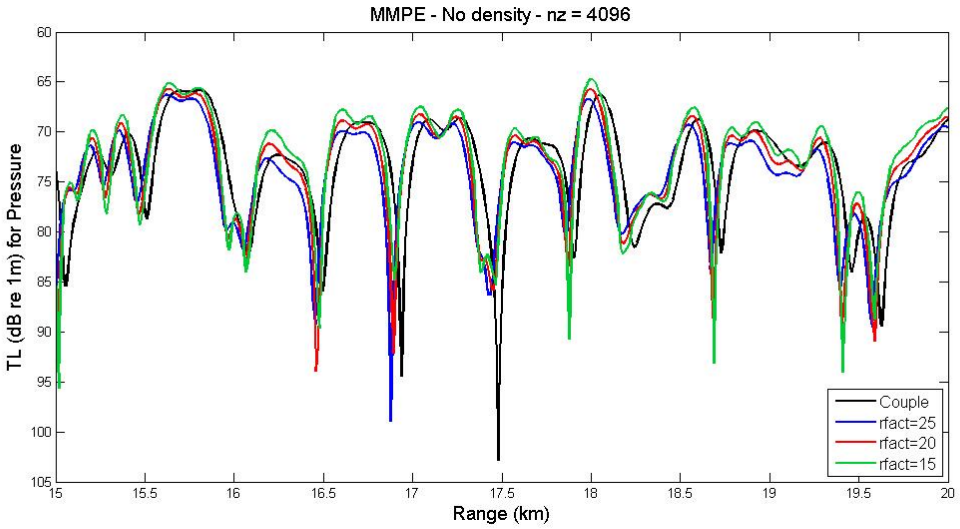

Figure 35. Closest approximation to benchmark solution, *nz* = 4096.

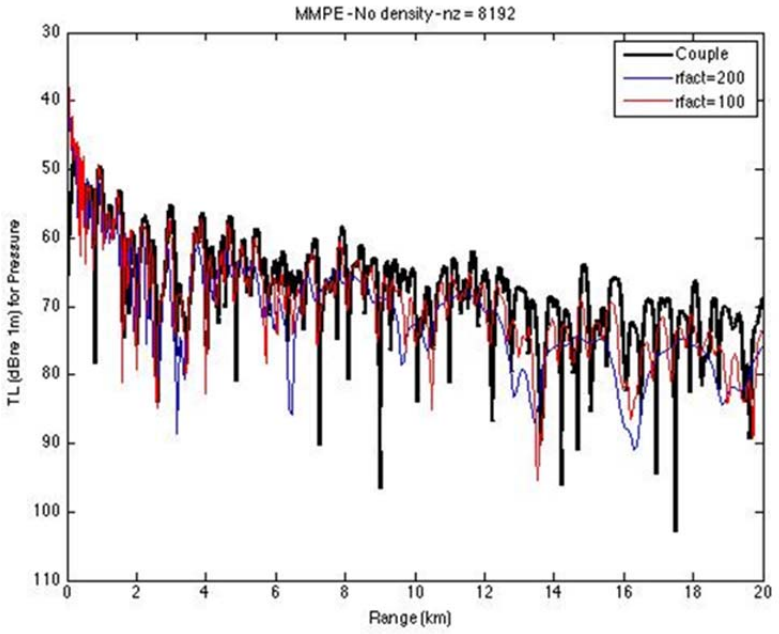

Figure 36. Original MMPE, no density, *nz* = 8192, *rfact* = 200, 100.

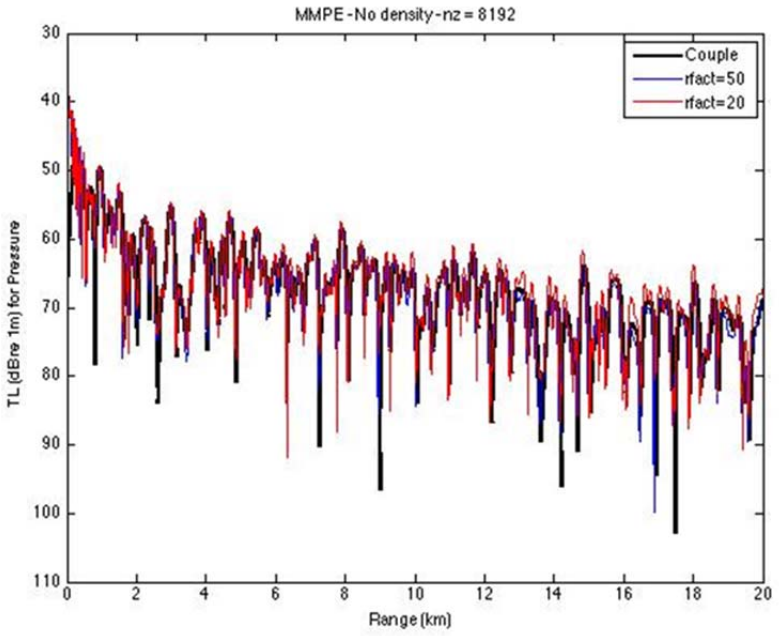

Figure 37. Original MMPE, no density, *nz* = 8192, *rfact* = 50, 20.

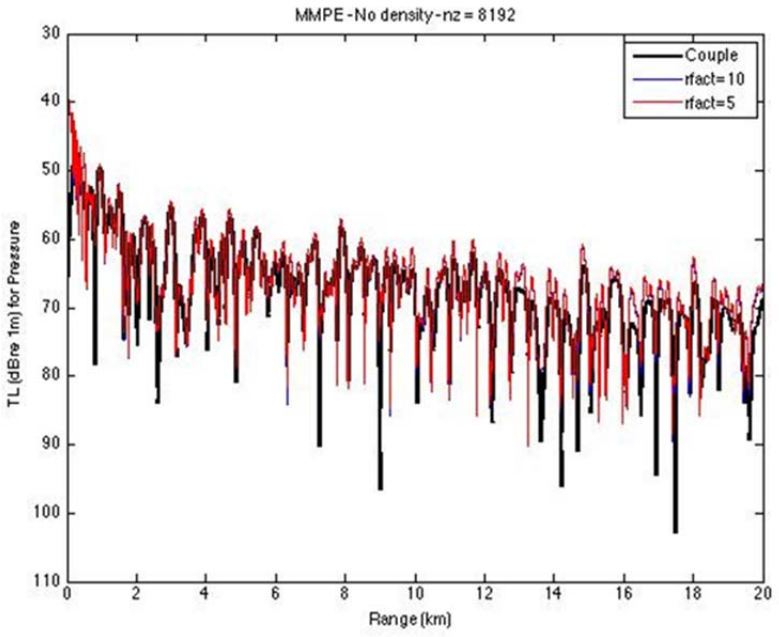

Figure 38. Original MMPE, no density, *nz* = 8192, *rfact* = 10, 5.

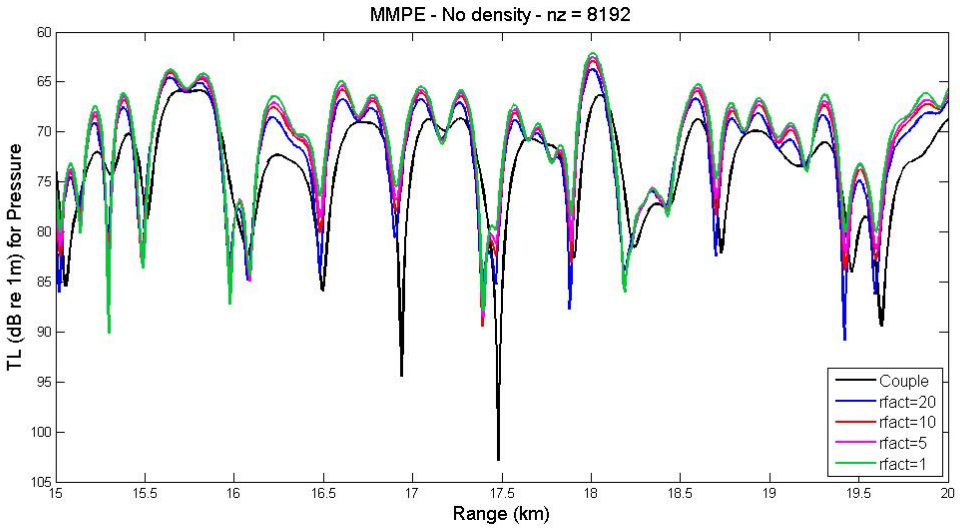

Figure 39. Solution convergence for *nz* = 8192.

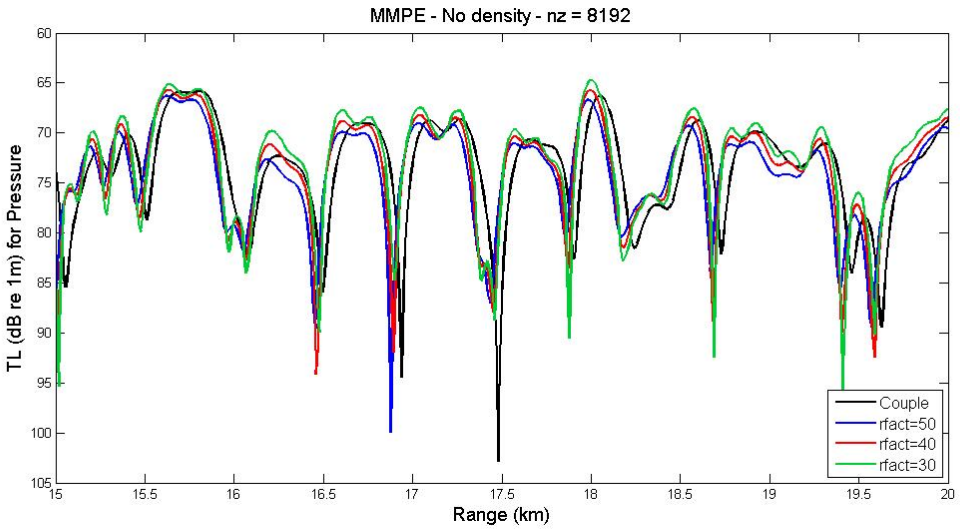

Figure 40. Closest approximation to benchmark solution, *nz* = 8192.

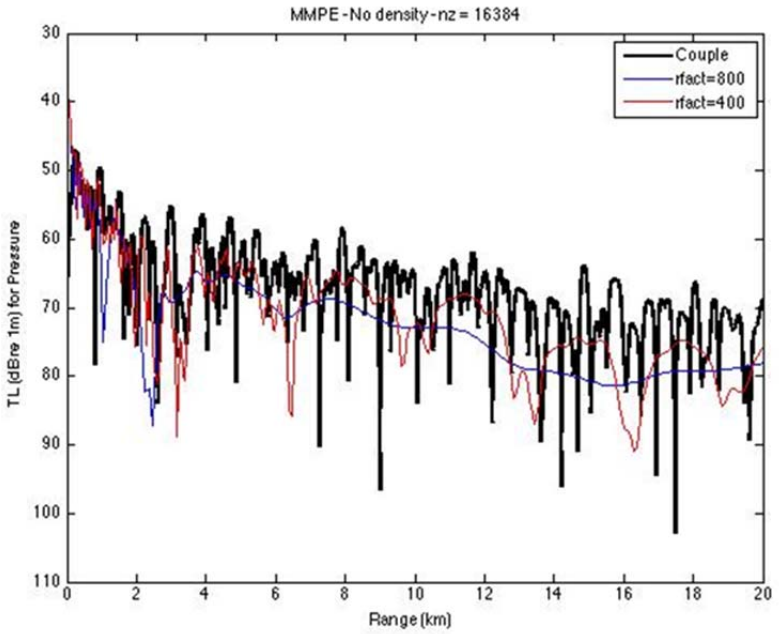

Figure 41. Original MMPE, no density, *nz* = 16,384, *rfact* = 800, 400.

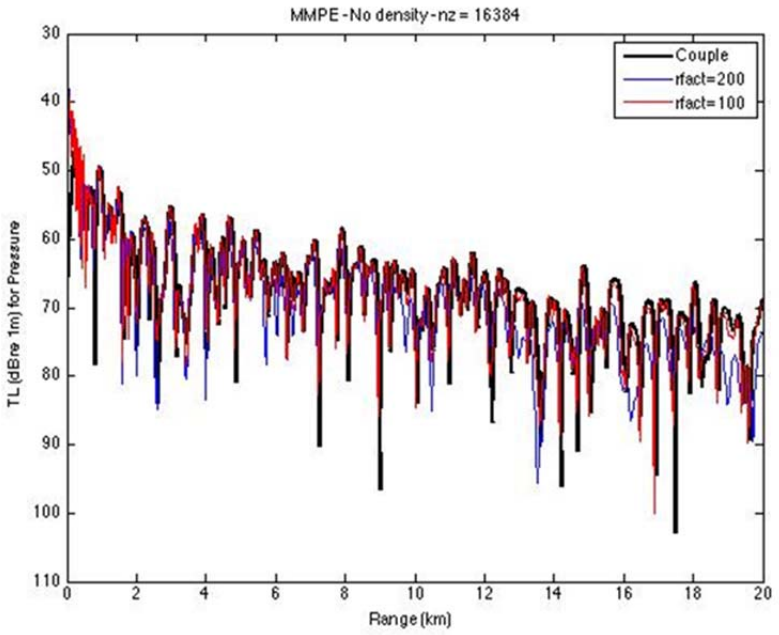

Figure 42. Original MMPE, no density, *nz* = 16,384, *rfact* = 200, 100.

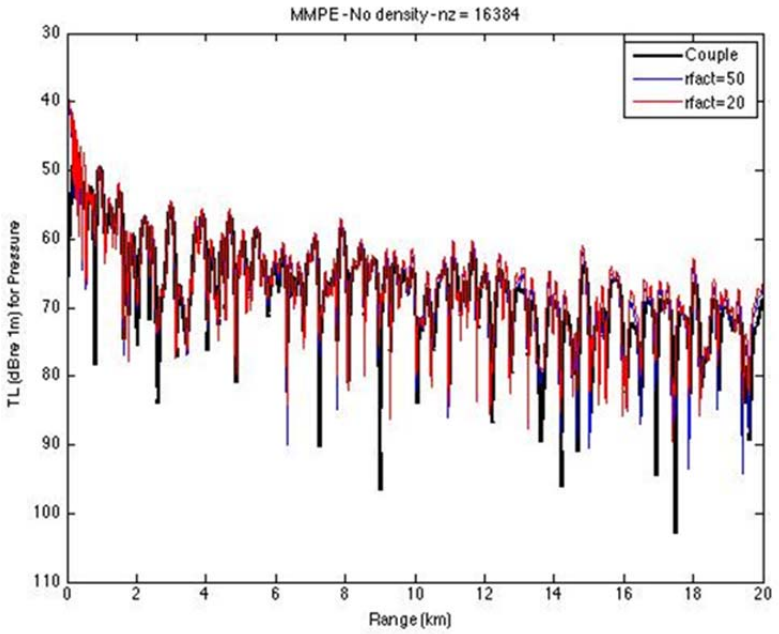

Figure 43. Original MMPE, no density, *nz* = 16,384, *rfact* = 50, 20.

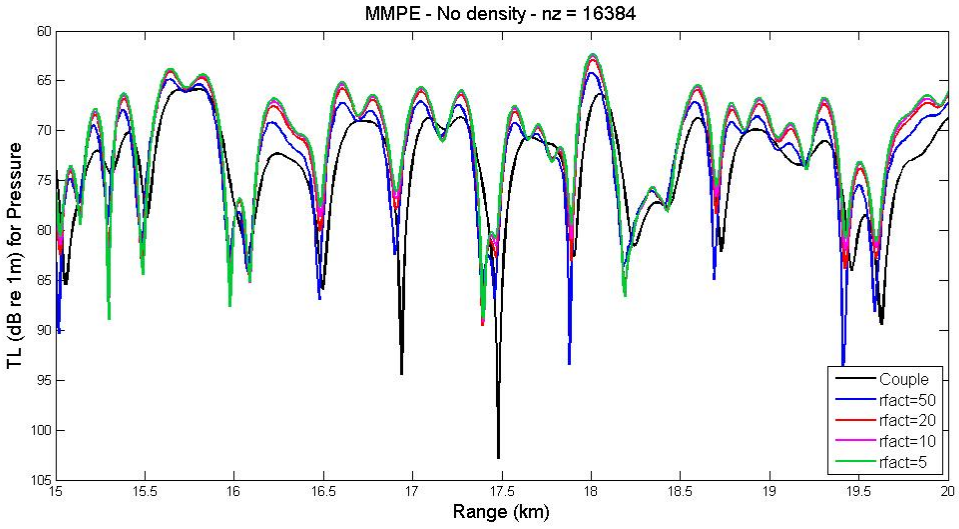

Figure 44. Solution convergence for *nz* = 16,384.

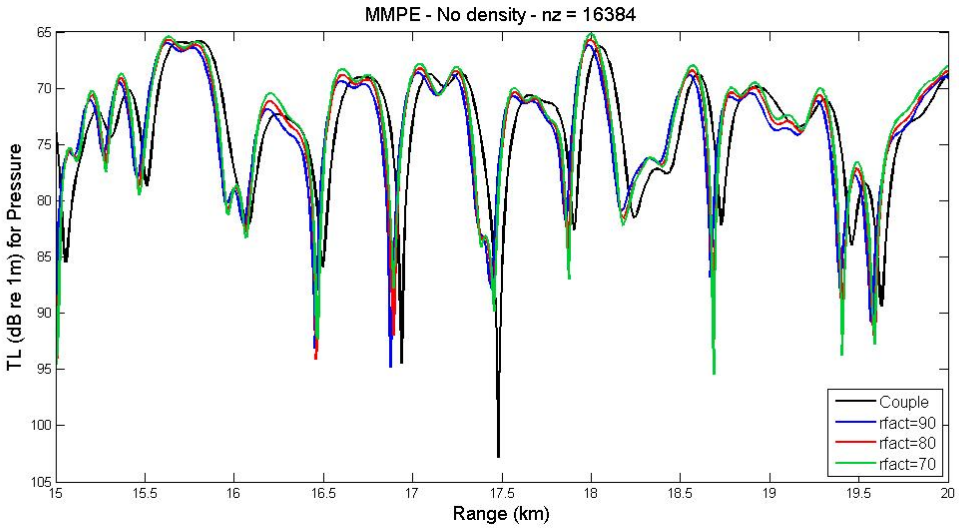

Figure 45. Closest approximation to benchmark solution, *nz* = 16,384.

THIS PAGE INTENTIONALLY LEFT BLANK

LIST OF REFERENCES

[1] F. D. Tappert, "The parabolic approximation method in underwater acoustics," *J. Acoust. Soc. Am.*, vol. 55, no. S1, pp. S34, Apr. 1974.

[2] R. H. Hardin and F. D. Tappert, "Applications of the split-step Fourier method to the numerical solution of nonlinear and variable coefficient wave equations," *SIAM*, vol. 15, no. 2, pp. 423, Apr. 1973.

[3] D. Lee and S. T. McDaniel, *Ocean Acoustic Propagation by Finite Difference Methods* (Pergamon, New York, 1988).

[4] M. D. Collins, "Applications and time-domain solutions of higher-order parabolic equations in underwater acoustics," *J. Acoust. Soc. Am.*, vol. 86, no. 2, pp. 1101–1102, Sep. 1989.

[5] D. Huang, "Finite element solution to the parabolic wave equation," *J. Acoust. Soc. Am.*, vol. 84, no. 4, pp. 1405–1413, Oct. 1988.

[6] F. B. Jensen *et al*, "Parabolic Equations," in *Computational Ocean Acoustics*, 2nd ed. New York: Springer-Verlag, 2011, pp. 457–529.

[7] J. A. Davis *et al*, *NORDA parabolic equation worshop*, Naval Ocean Research and Develpment Activity, Stennis Space Center, MS, 1982, pp.143.

[8] D. J. Thomson and N. R. Chapman, "A wide-angle split-step algorithm for the parabolic equation," *J. Acoust. Soc. Am.*, vol. 74, no. 6, pp. 1848–1854, Dec. 1983.

[9] F. D. Tappert, "The parabolic approximation method," in *Wave Propagation in Underwater Acoustics*, J. B. Keller and J. S. Papadakis, Eds. New York: Springer-Verlag, 1977, pp. 224–287.

[10] D. Yevick and D. J. Thomson, "A hybrid split-step/finite-difference PE algorithm for variable-density media," *J. Acoust. Soc. Am.* vol. 101, no. 3, pp. 1328–1335, Mar. 1997.

[11] K. B. Smith, "Convergence, stability, and variability of shallow water acoustic predictions using a split-step Fourier parabolic equation model," *J. Comput. Acous.*, vol. 9, no. 1, pp. 243–285, Apr. 2001.

[12] S. A. Chin-Bing *et al*., *PE Workshop II: Proceedings of the 2nd Parabolic Equation Workshop, May 6–9, 1991*, Naval Ocean Research and Develpment Activity, Stennis Space Center, MS, 1993.

[13] F. D. Tappert, "The c_0-Independent PE Model: Analysis of sound speed discontinuity," unpublished.

THIS PAGE INTENTIONALLY LEFT BLANK

INITIAL DISTRIBUTION LIST

1. Defense Technical Information Center
   Ft. Belvoir, Virginia

2. Dudley Knox Library
   Naval Postgraduate School
   Monterey, California